5 Melting

Most shaping operations consist of the flow and deformation of *heat-softened* or *melted* polymers; hence, the preparation of the polymer for the shaping operation generally includes a ''heating'' or ''melting'' step. In either case, we define the process of bringing polymers, commonly in particulate form, from the feed temperature to the desired processing temperature range, appreciably above the glass transition temperature, T_g, for amorphous polymers and above the melting point, T_m, for semicrystalline polymers, as the *elementary step of melting*.

The thermal energy requirements to achieve melting can be estimated from the specific enthalpy curves shown in Fig. 5.1. The area under any given curve represents the thermal energy needed to heat or melt one unit mass of that polymer from room to any higher temperature.

We note that semicrystalline polymers, where the ''break'' points are indicative of T_m, require more energy because they must undergo the phase transition of fusion. For example, about 700 kJ/kg are needed to heat HDPE to 200°C, while for the same processing temperature PS requires about 350 kJ/kg, that is, half the energy.

Melting of particulate solids has received relatively little attention in the classic engineering literature, probably because it is rarely a rate-limiting operation. Nevertheless, Ross (1) in the 1950s did offer a systematic classification of melting methods of fusible solids, though none of them is applicable to polymeric solids. However, melting in polymer processing *is* a very important elementary step, not only because it is often the *rate-controlling* step, which consumes 70–80% of the total processing energy input, but also because it determines to a large extent the product quality related to homogeneity and stability (e.g., injection-molding quality and film-thickness variation, respectively). Additionally, during melting of polymer blends, a major part of the *blend morphology* is being established.

In this chapter we elucidate the physical mechanisms of melting, demonstrate some of the common mathematical tools used in solving them, and demonstrate how these

Principles of Polymer Processing, Second Edition, by Zehev Tadmor and Costas G. Gogos.

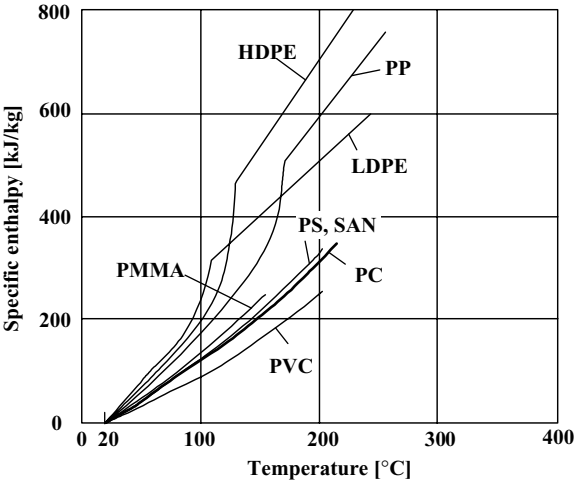

Fig. 5.1 Specific enthalpy curves for some common polymers.

mechanisms, in conjunction with inherent physical properties of polymers, lead to certain geometrical configurations of melting.

After the polymer has been shaped into the desired form, we are faced with the solidification problem (i.e., the inverse of the melting problem). We will find that, some of the solution methods developed in this chapter with regard to melting, are also valid for solidification.

5.1 CLASSIFICATION AND DISCUSSION OF MELTING MECHANISMS

The physical mechanisms that can bring about melting or heating of any substance are included in the terms of the thermal energy balance, Eq. 2.9-14

$$\rho \frac{Du}{Dt} = -\boldsymbol{\nabla} \cdot \mathbf{q} - P(\boldsymbol{\nabla} \cdot \mathbf{v}) - (\boldsymbol{\tau} : \boldsymbol{\nabla}\mathbf{v}) + \dot{S} \tag{5.1-1}$$

In Eq. 5.1-1 we added an additional possible homogeneous energy source $\dot{S}$ (e.g., dielectric heating). Clearly, the equation indicates four alternative sources by which the internal energy of a material can be raised, originating from each one of the terms on the right-hand side of the equation: (a) $(-\boldsymbol{\nabla} \cdot \mathbf{q})$, which is the net rate of internal energy increase per unit volume from an outside source by *heat conduction*; (b) $P(\boldsymbol{\nabla} \cdot \mathbf{v})$, which is the (reversible) rate of internal energy increase per unit volume by *compression*; (c) $[-(\boldsymbol{\tau} : \boldsymbol{\nabla}\mathbf{v})]$, which is the (irreversible) rate of internal energy increase by *flow* and *deformation*; and (d) $\dot{S}$, which is a possible external source for *homogeneous internal energy increase* such as dielectric heating. We can also include in such a term exothermic chemical reaction (although this emerges from an appropriately defined internal energy) and ultrasonic heating (although this can also be accounted for by the deformation term).

Let us now discuss, in physical terms, how important each of the previously discussed mechanisms is to the melting of polymers, and the limitations or advantages of each one due to the physical nature of polymers.

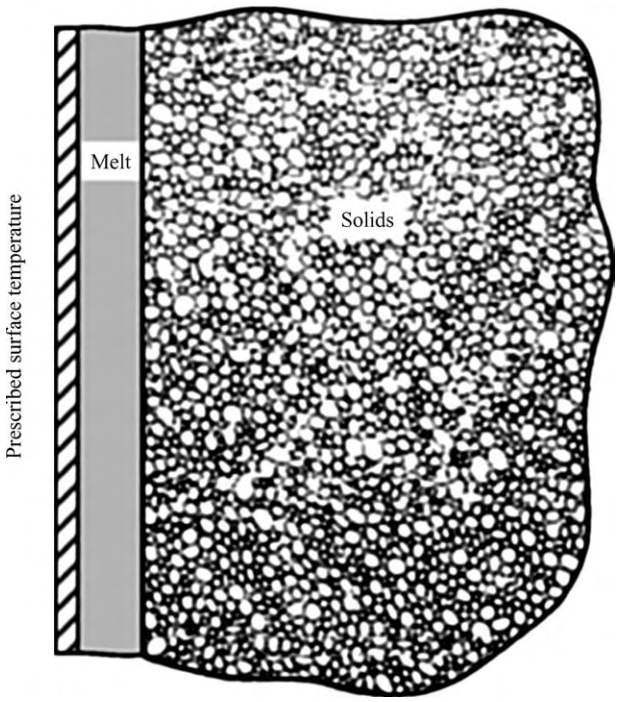

Fig. 5.2 Schematic representation of melting compacted polymeric solids by an outside heat source. A melt layer is formed which grows with time.

Conduction Melting

Conduction melting is the most common mode of raising the temperature of a solid and melting it. The surface temperature of a solid polymer or that of a compacted bed is raised by contact with a hot, solid surface, as shown in Figure 5.2.

As a result of this contact, a molten layer of polymer is formed, which grows with time. The mechanism of this kind of melting can be termed *conduction melting without melt removal.* The rate-controlling factors are the thermal conductivity, the attainable temperature gradients, and the available contact area between the heat source and the melting solid, reflecting material, operational, and configurational constraints, respectively. Thus, the low thermal conductivity of polymers (polymers are thermal insulators) and their temperature sensitivity (which makes them subject to thermal degradation and limits the attainable temperature gradients) place upper limits on the heat fluxes that can be applied.

Example 5.1 Thermal Degradation Characterization Thermal degradation is characterized by two temperature-dependent parameters, the *induction time* θ (T) for the onset of degradation, as shown in Fig. E5.1(a) for unplasticized Polyvinyl chloride (PVC), and the *rate of degradation*. The latter is shown in Fig. E5.1(b) in terms of the rate of change of the consistency index of the Power Law parameter, as a function of time and temperature, and can be expressed by the following equations:

$$m(t) = m_0 \qquad t \leq \theta(T)$$
$$m(t) = m_0 \exp[Ct \exp^{-\Delta E/RT}] \qquad t > \theta(T)$$

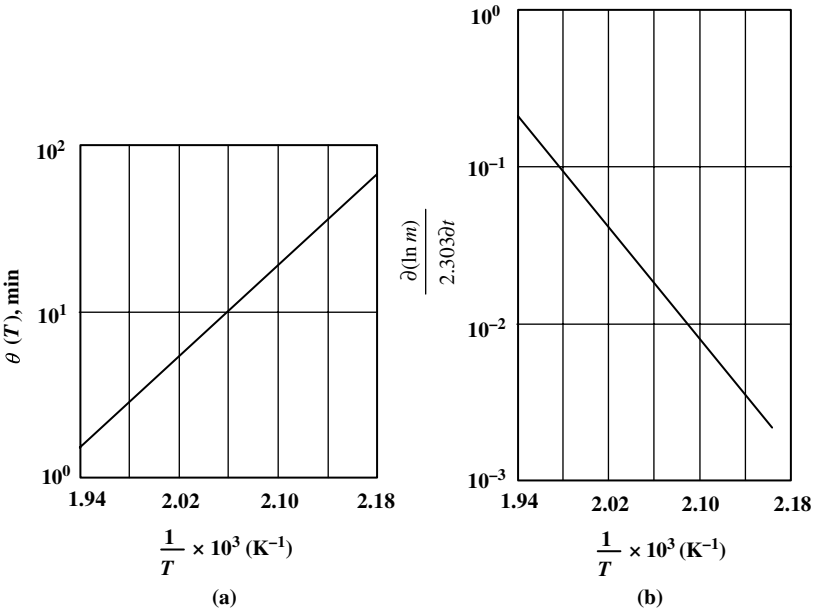

Fig. E5.1 Parameter reflecting thermal degradation of unplasticized PVC, Geon 101 EP-F24, as indicated by the time dependence of the consistency index m of the Power Law fluid model. [Reprinted by permission from E. A. Collins, B. F. Goodrich Chemical Co., Avon Lake, Ohio. Paper presented at the 1965 Society of Plastics Engineers Annual National Technical Conference, March 1966.]

Because of these limitations, and in particular because of the fact that, in such a mechanism, the temperature gradient at the wall that determines the heat flux to the solids drops exponentially with time, this melting mechanism is rather inefficient. However, the latter drawback can be alleviated if some mechanism continuously removes the molten layer. This, as shown in Fig. 5.3, can be accomplished either by applying a force normal to the heated surface, forcing out the melt by pressure flow, or by having the contact surface move parallel to its plane, dragging away the molten layer. These comprise the two

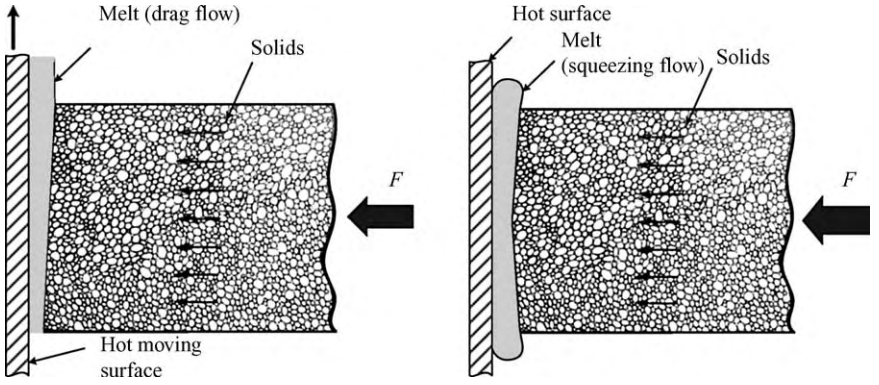

Fig. 5.3 Schematic representation of drag-induced melt removal and pressure-induced melt removal mechanisms.

melting mechanisms of *conduction melting with pressure-induced melt removal* and *drag-induced melt removal*, respectively.

"Grid melters" take advantage of the former mechanism and single screw extruders (SSEs), of the latter. In the elegant drag-removal melting mechanism that takes place in SSEs, significant temperature gradients can be maintained over thin films of melt, which not only quickly removes the freshly molten material from the vicinity of the high temperature zone and reduces the risk of degradation but also generates heat via viscous dissipation, further increasing the efficiency of melting. Moreover, in SSEs, the velocity of the moving solid plane or "wall" is tantamount to screw speed, and it becomes an important operating variable controlling the melting rate. Later in this chapter, we derive mathematical models for all these melting mechanisms.

Compressive Melting

Polymer solids and melts are virtually incompressible, and therefore very high pressures are needed for the term $P\,(\boldsymbol{\nabla}\cdot\mathbf{v})$ to assume reasonable values. Nevertheless, Menges and Elbe (2) demonstrated the feasibility of an injection molding process based on this mode of melting.

Deformation Melting

For viscous liquids the $[-(\boldsymbol{\tau}:\boldsymbol{\nabla}\mathbf{v})]$ term in Eq. 5.1-1 equals $(\boldsymbol{\tau}:\dot{\boldsymbol{\gamma}})/2$ and expresses the viscous energy dissipation (VED) per unit volume due to friction. The expression of the scalar product of the two tensors is given in the various coordinate systems in Table 2.5. For Newtonian fluids, this term further simplifies to $\mu(\dot{\boldsymbol{\gamma}}:\dot{\boldsymbol{\gamma}})/2$, and is given in the various coordinate systems in Table 2.6. Clearly, this term may be quite significant, because the viscosity of polymeric melts and the shear rates under processing conditions are high. As this term indicates, most polymeric melt flows are nonisothermal. Yet it also represents an important source of heat energy in drag-removal conduction melting, because of the very high shear rates imposed on the thin films in this melting mechanism. In fact, SSEs can be operated adiabatically with all the heat energy for melting originating in viscous dissipation.

As in viscous liquids, solid deformation also leads to irreversible conversion of mechanical energy to heat. In solids, however, deformation must exceed the elastic limit, and the imposed mechanical energy that is not elastically recovered is irreversibly dissipated into heat energy. In the melting step of polymer processing, we deform not a single piece of homogeneous solid polymeric body, but rather *repeated* deformation is imposed on a compacted bed of particulate solids. This generates significant, though nonhomogeneous, *heat energy* throughout the actively deformed bed via two distinct mechanisms: (a) individual polymeric particles undergo repeated deformations, generating heat within the particle, which we define as *plastic energy dissipation* (PED) (3), and (b) mechanical energy is dissipated into heat via interparticle friction, which we define as *frictional energy dissipation* (FED) (3). The compacted bed of solids cannot, of course, be considered a "continuum," and neither of these heat sources is uniform and homogeneous throughout the bed. Yet, as a *first* approximation for such "active" compacted polymer particulates and assemblies undergoing plastic deformations, we can add two source terms to the equation of thermal energy (Eq. 2.9-16), yielding:

$$\rho_s C_s \frac{DT}{Dt} = -\boldsymbol{\nabla}\cdot\mathbf{q} + \text{PED} + \text{FED} \tag{5.1-2}$$

The PED and FED terms are not easy to describe mathematically since, as pointed out earlier, they are not, strictly speaking, homogeneous sources within the compacted beds or particulate assemblies, which are made up of discrete bodies. Thus, friction takes place between *macroscopic* bodies, and even the deformation field *within* a single particle is nonhomogenous. Nevertheless, because of their *predominant role* in processing equipment, in particular in co-rotating twin screw extruders (TSEs), these melting sources provide a very effective deformation mix-melting mechanism. When molten polymer regions are formed due to PED and FED, and if the deforming stresses persist, then both PED and VED will act *simultaneously* as heat sources, resulting in a very effective mechanism of deformation mix-melting. We discuss this mechanism in more detail, and formulate it mathematically, in Section 5.8.

Homogeneous Internal Melting

Alternative heating mechanisms to conduction, such as dielectric or ultrasonic energies, have also been attempted. These mechanisms can be dissipated by polymer solids, creating volumewide homogeneous heat sources. With these mechanisms, the governing form of the thermal-energy balance becomes

$$\rho C_s \frac{\partial T}{\partial t} = -\nabla \cdot \mathbf{q} + \dot{S} \tag{5.1-3}$$

Although feasible, as shown by Erwin and Suh (4), using dielectric heating as an energy source is rather limited in polymer processing practice as a *primary* melting mechanism.

In summary, the melting mechanisms that are *effective* in melting polymers at acceptable rates, according to criteria of avoiding thermal degradation and achieving high processing rates, are summarized in Fig. 5.4a as

1. *Conduction melting with forced melt removal*, where both conduction and melt flow–induced VED achieve appreciable melting rates. This is the *primary* melting mechanism in *single rotor* polymer processing equipment. Such equipment, for example, SSEs and injection molding machines, are primarily forming devices, with the large pumping capabilities needed for forming; single-rotor devices allow the compacted polymer particulates to remain *passive*, without participating in the melting process.
2. *Plastic energy dissipation and frictional energy dissipation*, in that order of importance, where compacted polymer particulates are ''relentlessly'' deformed by *twin rotor devices*, which rapidly raise their temperature and create regions of melts.
3. *Dissipative mix-melting* (DMM), which becomes the operative melting mechanism *after* PED and FED have created a solids-rich melt suspension. In this early two-phase stage, PED may still be dominant. Soon afterwards, as melt-rich suspensions are created, VED becomes the dominant mechanism capable of rapidly eliminating all solids regions. Again *twin rotor co-* and *counterrotating* devices can cause the solid particulate assemblies to deform rapidly and repeatedly, enlisting them in the melting process. This is the reason that such devices are used when uniform and very rapid melting is required, as in postreactor polymer ''finishing'' operations.

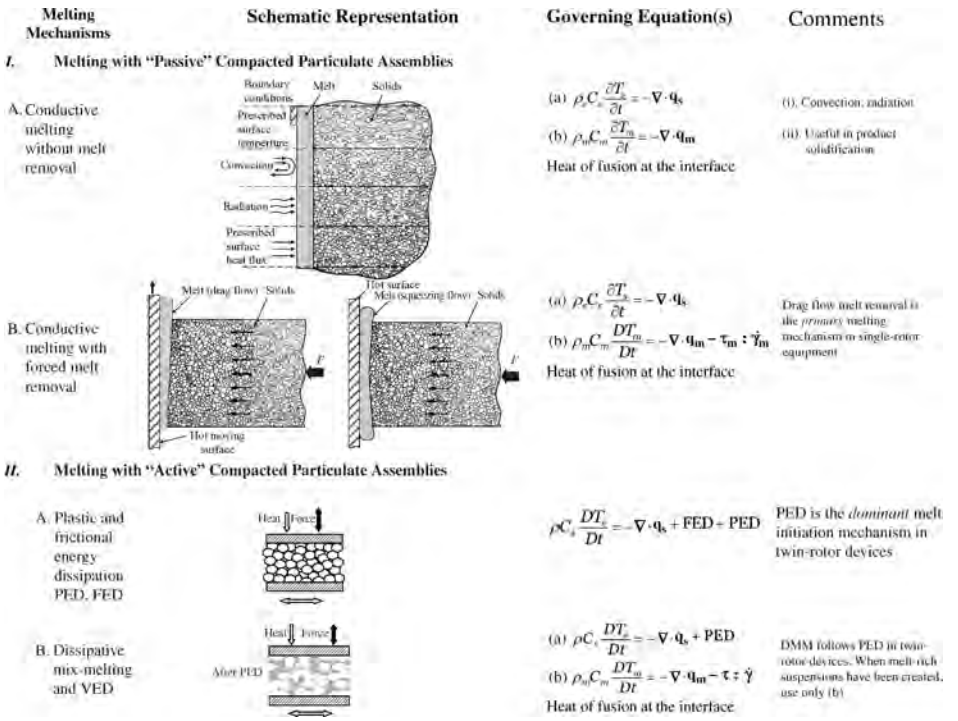

Fig. 5.4 Summary of the main mechanisms of the elementary step of melting. (I) Reprinted from Z. Tadmor and C. G. Gogos, *Principles of Polymer Processing*, Wiley, New York, 1979. (II) Reprinted by permission from C. G. Gogos, Z. Tadmor and M. H. Kim, ''Melting Phenomena and Mechanisms in Polymer Processing Equipment,'' *Adv. Polym. Technology,* **17**, 285–305 (1998).

5.2 GEOMETRY, BOUNDARY CONDITIONS, AND PHYSICAL PROPERTIES IN MELTING

To solve a heat transfer problem in polymer processing, the geometrical boundaries over which heat transfer takes place must be defined, boundary conditions selected, and the nature of the physical properties of the polymer specified.

Although melting in polymer processing may take place in geometrically complex machinery, the rate-determining step can often be modeled in terms of simple geometries, such as semi-infinite bodies, infinite flat slabs, and thin films. Analytical techniques prove to be useful in many of these cases. In solidification, on the other hand, the geometry of the frequently complex finished product coincides with the geometrical boundaries of the heat transfer problem, necessitating the application of *numerical* techniques.

The most important boundary condition in heat transfer problems encountered in polymer processing is the constant surface temperature. This can be generalized to a *prescribed surface temperature* condition, that is, the surface temperature may be an arbitrary function of time $T(0, t)$. Such a boundary condition can be obtained by direct contact with an external temperature-controlled surface, or with a fluid having a large heat transfer coefficient. The former occurs frequently in the heating or melting step in most

processing machinery, whereas the latter may be the case in cooling and solidifying, such as in the water trough solidification of extruded products.

A *prescribed surface convection* condition mathematically is stated as

$$h[T_a(t) - T(0,t)] = -k\frac{\partial}{\partial x}T(0,t) \tag{5.2-1}$$

where $T_a(t)$ is the ambient fluid temperature, and h is the heat transfer coefficient. The exposed surface temperature, $T(0,t)$, is another common boundary condition in heat transfer; in polymer processing, for example, we find it in air cooling of blown films, in oven heating of sheets prior to vacuum forming, in cooling of finished injection molding products, and in many other applications.

Yet another boundary condition encountered in polymer processing is *prescribed heat flux*. Surface-heat generation via solid–solid friction, as in frictional welding and conveying of solids in screw extruders, is an example. Moreover, certain types of intensive radiation or convective heating that are weak functions of surface temperature can also be treated as a prescribed surface heat-flux boundary condition. Finally, we occasionally encounter the highly nonlinear boundary condition of *prescribed surface radiation*. The exposure of the surface of an opaque substance to a radiation source at temperature T_r leads to the following heat flux:

$$\sigma\mathscr{F}[T_r^4 - T^4(0,t)] = -k\frac{\partial}{\partial x}T(0,t) \tag{5.2-2}$$

where $\sigma = 5.6697 \times 10^{-8}\,\mathrm{W/m^2\ K^4}$ $[1.712 \times 10^{-9}\,\mathrm{Btu/h\,ft^2\,{}^\circ R^4}]$ is the Stefan–Boltzmann radiation constant, and $\mathscr{F}$ is the combined configuration-emissivity factor. As pointed out earlier, if $T_r \gg T$, the boundary condition Eq. 5.2-2 reduces to a constant-flux condition.

In the melting process, amorphous polymers undergo a second-order transition and change from brittle to rubbery solids at the glass transition temperature, T_g. Although T_g is reported as a single temperature value, the transition actually takes place over a temperature range of the order of 5–10 °C. The value of T_g increases with increasing heating rate and applied hydrostatic pressure. Amorphous solids gradually become more deformable as they approach T_g, become "rubberlike" at $T_g < T < T_g + 100°\mathrm{C}$, known as the "rubbery plateau" region, and become fluidlike at $T > T_g + 100°\mathrm{C}$, called the *flow* (terminal) region. The crystalline portion of semicrystalline polymers, on the other hand, undergoes a first-order transition from the solid to the liquid state, with a characteristic heat of fusion λ, at the melting point T_m. Melting of the crystallites occurs over a 10–30°C range, depending on the spectrum of their sizes and perfection level, and on the rate of heating. The reported value of T_m is the temperature value at the *end* of this process; it depends on the polymer structure and, in the case of random copolymers, on the copolymer composition. Block copolymers exhibit the melting temperature characteristic of each of the two homopolymers.

Above T_m, the viscosity of the melt has Arrhenius-type dependence, decreasing (exponentially) with increasing temperature. Therefore a sharp transition is observed in both mechanical and viscous properties of semicrystalline polymers at T_m, resulting in a physical situation that is closer to the classic melting interface of monomeric crystals where, on one side, there is a viscous liquid, and on the other side, an elastic solid.

The physical and thermophysical properties of density, thermal conductivity, and specific heat are temperature dependent. It is a reasonably good approximation to use constant values for both the solid and molten states.

5.3 CONDUCTION MELTING WITHOUT MELT REMOVAL

As pointed out in the previous section, melting can often be modeled in terms of simple geometries. Here we analyze the transient conduction problem in a semi-infinite solid. We compare the solutions of this problem, assuming first (a) constant thermophysical properties, then (b) variable thermophysical properties and finally, and (c) a phase transition with constant thermophysical properties in each phase. These solutions, though useful by themselves, also help demonstrate the profound effect of the material properties on the mathematical complexities of the solution.

The equation of thermal energy (Eq. 2.9-16) for transient conduction in solids without internal heat sources reduces to

$$\rho C_\rho \frac{\partial T}{\partial t} = \nabla \cdot k \nabla T \tag{5.3-1}$$

If the thermal conductivity k and the product ρC_p are temperature independent, Eq. 5.3-1 reduces for homogeneous and isotropic solids to a linear partial differential equation, greatly simplifying the mathematics of solving the class of heat transfer problems it describes.[1]

Example 5.2 Semi-infinite Solid with Constant Thermophysical Properties and a Step Change in Surface Temperature: Exact Solution The semi-infinite solid in Fig. E5.2 is initially at constant temperature T_0. At time $t = 0$ the surface temperature is raised to T_1. This is a one-dimensional transient heat-conduction problem. The governing parabolic differential equation

$$\frac{\partial T}{\partial t} = \alpha \frac{\partial^2 T}{\partial x^2} \tag{E5.2-1}$$

where α is the thermal diffusivity, must be solved to satisfy the following initial and boundary conditions $T(x, 0) = T(\infty, t) = T_0$ and $T(0, t) = T_1$. Introducing a new variable[2] η combines the two independent variables x and t as follows:

$$\eta = Cxt^m \tag{E5.2-2}$$

1. For heat conduction in nonisotropic solids, see Ref. 5.

2. This transformation follows from general similarity solution methods, and is a similarity transformation. The term ''similar'' implies that profiles of the variable $T = T(x, t)$ (at different coordinates x) differ only by a scale factor. The profiles can be reduced to the same curve by changing the scale along the axis of ordinates. Problems that lack a ''characteristic length'' are generally amenable to this solution method.

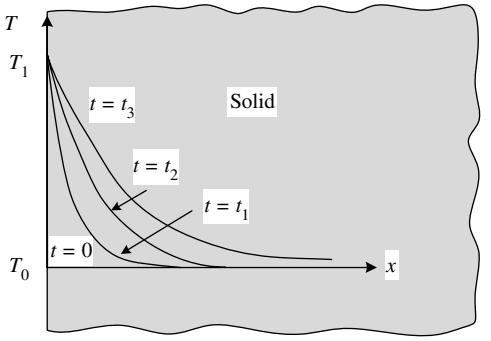

Fig. E5.2 Temperature profiles in a semi-infinite solid with a step change in temperature at the boundary.

where C and M are constants to be determined. Inserting Eq. E5.2-2 into Eq. E5.2-1 results in

$$m\eta\frac{dT}{d\eta} = \alpha C^2 t^{2m+1}\frac{d^2T}{d\eta^2} \tag{E5.2-3}$$

For Eq. E5.2-3 to be independent of t, the following equality must hold: $2m + 1 = 0$ or $m = -1/2$. Thus, the following ordinary differential equation is obtained

$$\frac{d^2T}{d\eta^2} + \frac{1}{2\alpha C^2}\eta\frac{dT}{d\eta} = 0 \tag{E5.2-4}$$

Next we let $C = 1/\sqrt{4\alpha}$, which further simplifies Eq. E5.2-4 to

$$\frac{d^2T}{d\eta^2} + 2\eta\frac{dT}{d\eta} = 0 \tag{E5.2-5}$$

Equation E5.2-5 can be easily solved by introducing another variable of transformation, $y = dT/d\eta$. The resulting temperature distribution is

$$T = C_1\frac{\sqrt{\pi}}{2}\text{erf}(\eta) + C_2 \tag{E5.2-6}$$

where

$$\eta = \frac{x}{\sqrt{4\alpha t}} \tag{E5.2-7}$$

and erf (z) is the well-known ''error function'' defined as

$$\text{erf}(z) = \frac{2}{\sqrt{\pi}}\int_0^z e^{-s^2}\,ds \tag{E5.2-8}$$

The constants C_1 and C_2 are obtained from the boundary conditions. Thus, boundary condition $T(0,t) = T_1$ is satisfied if $C_2 = T_1$ whereas both conditions $T(x,0) = T(\infty,t) = T_0$ imply $T = T_0$ at $\eta \to \infty$ (which is the direct result of the combination of variables). Thus we get $C_1 = 2(T_0 - T_1)/\pi^{1/2}$. Substituting these values into Eq. E5.2-6 results in

$$\frac{T - T_1}{T_0 - T_1} = \text{erf}(\eta) \tag{E5.2-9}$$

which satisfies both the differential equation and the boundary conditions, and hence is a solution to the problem.

The heat flux into the solid is obtained by differentiating Eq. E5.2-9 with respect to x, and using Fourier's law

$$q_x = -k\left(\frac{\partial T}{\partial x}\right)_{x=0} = -k\left[\frac{T_0 - T_1}{\sqrt{\pi\alpha t}} e^{-\eta^2}\right]_{x=0} = \frac{k}{\sqrt{\pi\alpha t}}(T_1 - T_0) \tag{E5.2-10}$$

The results so far are both interesting and significant. First, we have obtained a particular dimensionless combination of the key variables: distance, time, and thermal diffusivity in Eq. E5.2-7, and the temperature profile becomes a unique function of this single dimensionless variable η.

We shall see later that this combination of the key variables is also characteristic of conduction heating with phase transfer. The heat flux is infinite at $t = 0$, but quickly drops with the inverse of $t^{1/2}$. Thus after 10 s it is only 30% of the flux at 1 s, and after 60 s, it is only 13% of the heat flux at 1 s! The obvious conclusion is that conduction melting without melt removal becomes inefficient for anything but short times.

Example 5.3 The Semi-infinite Solid with Variable Thermophysical Properties and a Step Change in Surface Temperature: Approximate Analytical Solution We have stated before that the thermophysical properties (k, ρ, C_p) of polymers are generally temperature dependent. Hence, the governing differential equation (Eq. 5.3-1) is nonlinear. Unfortunately, few analytical solutions for nonlinear heat conduction exist (5); therefore, numerical solutions (finite difference and finite element) are frequently applied. There are, however, a number of useful *approximate analytical* methods available, including the integral method reported by Goodman (6). We present the results of Goodman's approximate treatment for the problem posed in Example 5.2, for comparison purposes.

We begin with Eq. 5.3-1 and introduce a variable of transformation for T

$$d\Theta(x,t) = \rho C_p \, dT \tag{E5.3-1}$$

or in integrated form:

$$\Theta(x,t) = \int_{T_0}^{T} \rho C_\rho \, dT \tag{E5.3-2}$$

where Θ is the heat added per unit volume at location x and time t. Substituting Eq. E5.3-1 into Eq. 5.3-1 gives

$$\frac{\partial \Theta}{\partial t} = \frac{\partial}{\partial x}\alpha(\Theta)\frac{\partial \Theta}{\partial x} \tag{E5.3-3}$$

Next we integrate Eq. E5.3-3 over x from the outer surface ($x = 0$) to a certain, yet unknown depth $\delta(t)$, which is defined as the *thermal penetration depth*

$$\int_0^{\delta} \frac{\partial \Theta}{\partial t} dx = \int_0^{\delta} \left[\frac{\partial}{\partial x} \alpha(\Theta) \frac{\partial \Theta}{\partial x} \right] dx \tag{E5.3-4}$$

The penetration depth reflects the time-dependent distance from the surface to a location where thermal effects become negligible. Using the Leibnitz formula for the left-hand side of Eq. E5.3-4, we get

$$\frac{d}{dt} \int_0^{\delta} \Theta \; dx - \Theta(\delta, t) \frac{d\delta}{dt}$$

But $\Theta(\delta, t) = 0$, because we defined δ as the distance at which thermal effects fade away; that is we assume that $T(\delta) = T_0$. Thus, the right-hand side of Eq. E5.3-4 simply becomes

$$- \left[\alpha(\Theta) \frac{\partial \Theta}{\partial x} \right]_{x=0}$$

and Eq. 5.3-4 can be rewritten as

$$\frac{d}{dt} \int_0^{\delta} \Theta \, dx = - \left[\alpha(\Theta) \frac{\partial \Theta}{\partial x} \right]_{x=0} \tag{E5.3-5}$$

The advantage of the Goodman transformation is now apparent: the temperature-dependent thermophysical properties in the integrated differential equation have to be evaluated only at the surface temperature, T_1. The variation of the properties with the temperature appear in the boundary condition for $\Theta(x, t)$

$$\Theta(x, t) = \Theta_1 = \int_{T_0}^{T_1} \rho C_p \, dT \tag{E5.3-6}$$

Boundary conditions $T(x, 0) = T(\infty, t) = T_0$ are both taken care of by assuming a time-dependent thermal penetration depth of finite thickness.

Next we assume a temperature profile that a priori satisfies the boundary condition $\Theta(0, t) = \Theta_1, \Theta(\delta, 0) = 0$ and $(\partial \Theta / \partial x)_{x=\delta} = 0$, such as

$$\Theta = \Theta_1 \left(1 - \frac{x}{\delta} \right)^3 \tag{E5.3-7}$$

By substituting Eq. E5.3-7 into Eq. E5.3-5, the time dependence of δ is obtained

$$\delta = \sqrt{24 \alpha_1 t} \tag{E5.3-8}$$

where α_1 is α evaluated at T_1. For polymers with typical α values of $1 \times 10^{-7}\ \mathrm{m^2/s}$, the penetration depth is 1 mm after 1 s and 1 cm after 60 s.

From Eq. E5.3-7, we obtain

$$\Theta(x, t) = \Theta_1 \left(1 - \frac{x}{\sqrt{24 \alpha_1 t}} \right)^3 \tag{E5.3-9}$$

The temperature profile at any given time is obtained by calculating Θ for various x values ($0 < x < \delta$) and obtaining from Eq. E5.3-7 the corresponding temperatures. The latter, of course, requires knowing the temperature dependences of ρC_p.

For constant thermophysical properties Eq. E5.3-9 reduces to

$$\frac{T - T_0}{T_1 - T_0} = \left(1 - \frac{x}{\sqrt{24\alpha t}}\right)^3 \tag{E5.3-10}$$

The heat flux at $x = 0$ is

$$q_x = \frac{k}{\sqrt{8\alpha t/3}}(T_1 - T_0) \tag{E5.3-11}$$

which can be compared to the exact solution in Eq. E5.2-10, showing a small difference between the two solution methods. This difference depends on the selection of the trial function, and in this case it is 8%.

Example 5.4 Melting of a Semi-infinite Solid with Constant Thermophysical Properties and a Step Change in Surface Temperature: The Stefan–Neumann Problem The previous example investigated the heat conduction problem in a semi-infinite solid with constant and variable thermophysical properties. The present Example analyzes the same conduction problem with a change in phase.

Interest in such problems was first expressed in 1831 in the early work of G. Lamè and B. P. Clapeyron on the freezing of moist soil, and in 1889 by J. Stefan on the thickness of polar ice and similar problems. The exact solution of the phase-transition problem in a semi-infinite medium is due to F. Neumann (who apparently dealt with this kind of problem even before Stefan), and thus, problems of this kind are called Stefan–Neumann problems. The interest in these problems has been growing ever since (7,8).

The presence of a moving boundary between the phases introduces nonlinearity into the boundary conditions. Hence, there are only a few exact solutions, and we must frequently turn to approximate analytical or numerical solutions.

In this example, we consider the classic Stefan–Neumann solution. The solid is initially at a constant temperature T_0. At time $t = 0$ the surface temperature is raised to T_1, which is above the melting point, T_m. The physical properties of each phase are different, but they are temperature independent, and the change in phase involves a latent heat of fusion λ. After a certain time t, the thickness of the molten layer is $X_l(t)$; in each phase there is a temperature distribution and the interface is at the melting temperature T_m (Fig. E5.4).

Heat is conducted from the outer surface through the melt to the free interface, where some of the heat is absorbed as heat of fusion, melting some more solid, and the rest is conducted into the solid phase. The densities of melt and solid are usually different. We denote the melt phase with subscript l and the solid with subscript s. The thickness of the molten layer increases because of melting, and there is also a slight increase due to a decrease in density as the solid melts. If there were no decrease in density, the thickness of the molten layer would remain X_s. Thus, the relationship between X_l and X_s is given by

$$\frac{X_l}{X_s} = \frac{\rho_s}{\rho_l} = \beta \tag{E5.4-1}$$

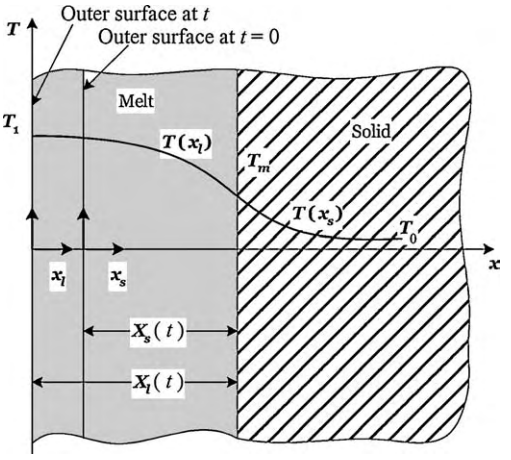

Fig. E5.4 Melting in a semi-infinite solid. $X_l(t)$ is the thickness of the molten layer at time t, $X_s(t)$ is the distance of the interface from the location of external surface at time $t = 0$. The temperature profile in the solid is expressed in coordinate x_s, which is stationary, whereas the temperature profile in the melt is expressed in coordinate x_l, which has its original outer surface of melt, hence, it slowly moves with time if $\rho_s \neq \rho_l$.

The governing differential equation in both phases is Eq. E5.2-1. For the melt phase, it takes the form

$$\frac{\partial^2 T_l}{\partial x_l^2} - \frac{1}{\alpha_l}\frac{\partial T_l}{\partial t} = 0 \tag{E5.4-2}$$

with boundary conditions $T_l(0,t) = T_1$ and $T_l(x_l,t) = T_m$.

It should be noted that the coordinate x_l has its origin at the outer surface of the melt which, if $\rho_s \neq \rho_l$. slowly moves with the melting process. For the solid phase we have

$$\frac{\partial^2 T_s}{\partial x_s^2} - \frac{1}{\alpha_s}\frac{\partial T_s}{\partial t} = 0 \tag{E5.4-3}$$

with the boundary conditions $T_s(\infty,t) = T_0$ and $T_s(x_s,t) = T_m$.

The coordinate x_s has its origin at the external surface when melting started, and it is stationary. In addition to the boundary conditions just given, we can write a heat balance for the interface (this is occasionally referred to as the Stefan condition).

$$\underbrace{k_l\left(\frac{\partial T_l}{\partial x_l}\right)_{x_l=X_l}}_{\substack{\text{Heat flux into}\\ \text{the interface}}} - \underbrace{k_s\left(\frac{\partial T_s}{\partial x_s}\right)_{x_s=X_s}}_{\substack{\text{Heat flux out}\\ \text{from interface}}} = \underbrace{\lambda\rho_l\frac{dX_l}{dt} = \lambda\rho_s\frac{dX_s}{dt}}_{\substack{\text{Rate of melting}\\ \text{per unit interface}}} \tag{E5.4-4}$$

We assume that the temperature profile in each phase has the form of the temperature profile in a semi-infinite solid with a step change in surface temperature as derived in Example 5.2. Thus we get the following temperature profiles for melt and solid phases, respectively,

$$T_l = T_1 + A\,\mathrm{erf}\left(\frac{x_l}{2\sqrt{\alpha_l t}}\right) \tag{E5.4-5}$$

which automatically satisfies the boundary condition $T_l(0,t) = T_1$, and

$$T_s = T_0 + B\,\mathrm{erf}c\left(\frac{x_s}{2\sqrt{\alpha_s t}}\right) \tag{E5.4-6}$$

where erfc $(s) = 1 - \mathrm{erf}(s)$, and which satisfies the boundary condition $T_s(\infty,t) = T_0$. Both equations must satisfy the boundary condition, stating that the temperature at the interface is that of the melting point:

$$T_m = T_1 + A\,\mathrm{erf}\left(\frac{X_l}{2\sqrt{\alpha_l t}}\right) \tag{E5.4-7}$$

$$T_m = T_0 + B\,\mathrm{erfc}\left(\frac{X_s}{2\sqrt{\alpha_s t}}\right) \tag{E5.4-8}$$

Now, Eqs. E5.4-7 and E5.4-8 must hold for all times t. This is possible *only* if both X_l and X_s are proportional to the square root of time. We can, therefore, write

$$X_s = K\sqrt{t} \tag{E5.4-9}$$

and with the aid of Eq. E5.4-1 we get

$$X_l = \beta K\sqrt{t} \tag{E5.4-10}$$

where K is an unknown constant. From Eqs. E5.4-9 and E5.4-10 we conclude, without even having the complete solution, that the thickness of the molten layer grows at a rate proportional to the square root of time. It is interesting to note the similarity between the penetration depth, as obtained in the preceding examples, and the location of the interface. This similarity suggests the application of approximate solution methods to phase-transition problems.

The constant K can be evaluated by substituting Eqs. E5.4-5 and E5.4-6 into Eq. E5.4-4. Subsequent to evaluating the constants A and B from the boundary conditions and Eqs. E5.4-9 and E5.4-10

$$\frac{(T_m - T_1)k_l e^{-K^2\beta^2/4\alpha_l}}{\sqrt{\pi\alpha_l}\,\mathrm{erf}(K\beta/2\sqrt{\alpha_l})} - \frac{(T_0 - T_m)k_s e^{-K^2/4\alpha_s}}{\sqrt{\pi\alpha_s}\,\mathrm{erfc}(K/2\sqrt{\alpha_s})} = \lambda\rho_l\frac{K\beta}{2} \tag{E5.4.11}$$

The root of this transcendental equation is K, and it is a function of the initial and boundary conditions, as well as the physical properties of the two phases. Tabulated solutions of Eq. E5.4-11 for $\beta = 1$ to four-digit accuracy are given by Churchill and Evans (9). The temperature profiles in the two phases are obtained from Eqs. E5.4-5 and E5.4-6, with the aid of Eqs. E5.4-7 and E5.4-8

$$\frac{T_l - T_m}{T_1 - T_m} = 1 - \frac{\mathrm{erf}(x_l/2\sqrt{\alpha_l t})}{\mathrm{erf}(K\beta/2\sqrt{\alpha_l})} \tag{E5.4-12}$$

and

$$\frac{T_s - T_m}{T_0 - T_m} = 1 - \frac{\mathrm{erfc}(x_s/2\sqrt{\alpha_s t})}{\mathrm{erfc}(K/2\sqrt{\alpha_s})} \tag{E5.4-13}$$

Equations E5.4-12 and E5.4-13 satisfy the differential equation and the boundary and initial conditions. Therefore they form an exact solution to the problem. In the preceding solution we neglected heat convection as a result of the expansion of the melt phase due to the density decrease. The rate of melting per unit area as a function of time can be obtained from Eq. E5.4-10

$$w_A = \rho_l \frac{dX_l}{dt} = \frac{\rho_s K}{2\sqrt{t}} \tag{E5.4-14}$$

Again we note the similarity in the solution of the conduction problem with constant thermophysical properties, to those with variable properties, and with phase transition. Clearly, the rate of melting drops with time as the molten layer, which essentially forms a thermal shield, increases in thickness. This result, once again, directs our attention to the advantage accruing from forced removal of the molten layer from the melting site. The average rate of melting is

$$\bar{w}_A = \frac{1}{t}\int_0^t \frac{\rho_s K}{2\sqrt{t}}\, dt = \frac{\rho_s K}{\sqrt{t}} \tag{E5.4-15}$$

The preceding examples discuss the heat-conduction problem without melt removal in a semi-infinite solid, using different assumptions in each case regarding the thermophysical properties of the solid. These solutions form useful approximations to problems encountered in everyday engineering practice. A vast collection of analytical solutions on such problems can be found in classic texts on heat transfer in solids (10,11). Table 5.1 lists a few well-known and commonly applied solutions, and Figs. 5.5–5.8 graphically illustrate some of these and other solutions.

Most real cases of polymer melting (and solidification) involve complex geometries and shapes, temperature-dependent properties, and a phase change. The rigorous treatment for such problems involve numerical solutions (12-15) using finite difference (FDM) or FEMs. Figure 5.9 presents calculated temperature profiles using the Crank–Nicolson FDM (16) for the solidification of a HDPE melt inside a flat-sheet injection-mold cavity. The HDPE melt that has filled the cavity is considered to be initially isothermal at 300°F, and the mold wall temperature is 100°F.

5.4 MOVING HEAT SOURCES

Conductive heating with moving heat sources was treated in detail by Rosenthal (17), particularly in relation to metal processing such as welding, machining, grinding, and continuous casting. In polymer processing, we also encounter heat conduction problems with moving heat sources as well as heat sinks. The commonly practiced welding of polyvinyl chloride, the continuous dielectric sealing of polyolefins, the heating of films and thin sheets under intense radiation lamps, and in certain cases, the heating or chilling of continuous films and sheets between rolls are some examples. These processes are usually steady or quasi–steady state, with heat introduced or removed at a point or along a line. We now examine one particular case to demonstrate the solution procedure.

TABLE 5.1 Analytical Solutions to Some Common Heat Transfer Problems (Constant Physical Properties)

Geometry	Initial and Boundary Conditions	Temperature Distribution
Semi-infinite solid	$T(x,0)=T_0 \quad T(0,t)=T_1 \quad T(\infty,t)=T_0$	$\dfrac{T-T_1}{T_0-T_1}=\operatorname{erf}\left(\dfrac{x}{\sqrt{4\alpha t}}\right)$
Semi-infinite solid	$T(x,0)=T_0 \quad T(\infty,t)=T_0 \quad -k\left(\dfrac{\partial T}{\partial x}\right)_{x=0}=q_0$	$T-T_0=\dfrac{q_0}{k}\sqrt{4\alpha t}\quad \text{iecrfc}\left(\dfrac{x}{\sqrt{4\alpha t}}\right)$
Flat plate	$T(x,0)=T_0 \quad T(\pm b,t)=T_1$	$\dfrac{T_1-T}{T_1-T_0}=2\sum_{n=0}^{\infty}\dfrac{(-1)^n}{(n+\frac{1}{2})\pi}e^{-\left(n+\frac{1}{2}\right)^2\pi^2(\alpha t/b^2)}\cos\left[\left(n+\dfrac{1}{2}\right)\pi\dfrac{x}{b}\right]$
Flat plate	$T(x,0)=T_0 \quad \left.\dfrac{-\partial T}{\partial x}\right\|_{x=-b}=\dfrac{h}{k}[T_1-T(-b)]$ $\left.\dfrac{-\partial T}{\partial x}\right\|_{x=b}=\dfrac{h}{k}[T(b)-T_1]$	$\dfrac{T_1-T}{T_1-T_0}=\sum_{n=1}^{\infty}\dfrac{2\left(\dfrac{hb}{k}\right)\cos\beta_n\left(\dfrac{x}{b}\right)}{\left[\beta_n^2+\dfrac{hb}{k}+\left(\dfrac{hb}{k}\right)^2\right]\cos\beta_n}e^{-\beta_n^2(\alpha t/b^2)} \qquad \beta_n\tan\beta_n=\dfrac{hb}{k}$
Cylinder	$T(r,0)=T_0 \quad T(R,t)=T_1$	$\dfrac{T_1-T}{T_1-T_0}=\dfrac{2}{R}\sum_{n=1}^{\infty}\dfrac{J_0(rc_n)}{c_nJ_1(Rc_n)}e^{-\alpha c_n^2 t}\,J_0(Rc_n)=0$
Cylinder	$T(r,0)=T_0 \quad -k\left(\dfrac{\partial T}{\partial r}\right)_{r=R}=h[T(R)-T_1]$	$\dfrac{T_1-T}{T_1-T_0}=\dfrac{2}{R}\sum_{n=1}^{\infty}\exp(-\alpha\beta_n^2t)\dfrac{\dfrac{h}{k}J_0(r\beta_n)}{\left[\left(\dfrac{h}{k}\right)^2+\beta_n^2\right]J_0(R\beta_n)} \qquad \beta_n\dot{J}_0(R\beta_n)+\dfrac{h}{k}J_0(R\beta_n)=0$
Sphere	$T(r,0)=T_0 \quad T(R,t)=T_1$	$\dfrac{T_1-T}{T_1-T_0}=\dfrac{2R}{\pi r}\sum_{n=1}^{\infty}\dfrac{(-1)^n}{n}\sin\dfrac{n\pi r}{R}e^{-\alpha n^2\pi^2t/R^2}$
Sphere	$T(r,0)=T_0 \quad -k\left(\dfrac{\partial T}{\partial r}\right)_{r=R}=h[T(R)-T_1]$	$\dfrac{T_1-T}{T_1-T_0}=\dfrac{2\frac{h}{k}}{r}\sum_{n=1}^{\infty}\exp(-\alpha\beta_n^2t)\dfrac{R^2\beta_n^2+\left[R\left(\dfrac{h}{k}\right)-1\right]^2}{\beta_n^2\left[R^2\beta_n^2+R\dfrac{h}{k}\left(R\dfrac{h}{k}-1\right)\right]}\quad \sin(R\beta_n)\sin(r\beta_n)$ $R\beta_n\cot(R\beta_n)+R\left(\dfrac{h}{k}\right)-1=0$

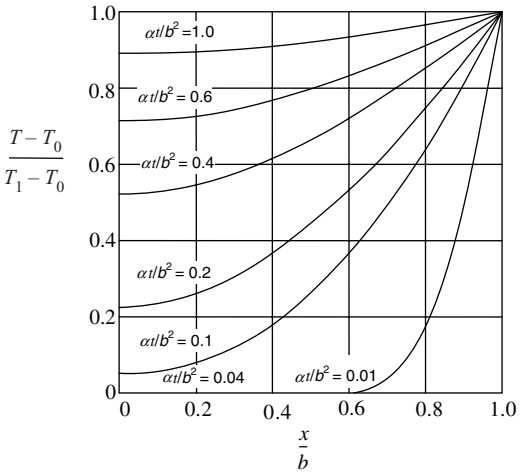

Fig. 5.5 Temperature profiles for unsteady-state heat conduction in finite flat plates: $T(x,0) = T_0, T(\pm b,t) = T_1$. [Reprinted by permission from H. S. Carslaw and J. C. Jaeger, *Conduction of Heat in Solids*, 2nd ed., Oxford University Press, New York, 1973.]

Example 5.5 Continuous Heating of a Thin Sheet Consider a thin polymer sheet infinite in the x direction, moving at constant velocity V_0 in the negative x direction (Fig. E5.5). The sheet exchanges heat with the surroundings, which is at $T = T_0$, by convection. At $x = 0$, there is a plane source of heat of intensity q per unit cross-sectional area. Thus the heat source is moving relative to the sheet. It is more convenient, however, to have the coordinate system located at the source. Our objective is to calculate the axial temperature profile $T(x)$ and the intensity of the heat source to achieve a given maximum temperature. We assume that the sheet is thin, that temperature at any x is uniform, and that the thermophysical properties are constant.

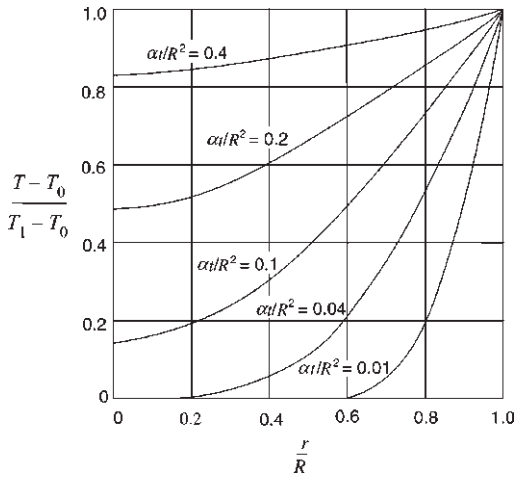

Fig. 5.6 Temperature profiles for unsteady-state heat conduction in infinite cylinders: $T(r,0) = T_0, T(R,t) = T_1$. [Reprinted by permission from H. S. Carslaw and J. C. Jaeger, *Conduction of Heat in Solids*, 2nd ed., Oxford University Press, New York, 1973.]

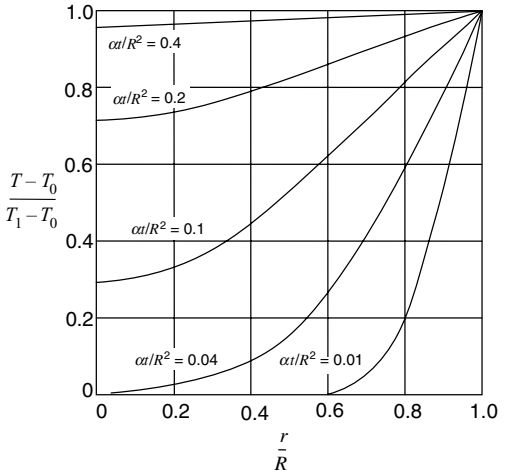

Fig. 5.7 Temperature profiles for unsteady-state heat conduction in spheres: $T(r, 0) = T_0$, $T(R, t) = T_1$. [Reprinted by permission from H. S. Carslaw and J. C. Jaeger, *Conduction of Heat in Solids*, 2nd ed., Oxford University Press, New York, 1973.]

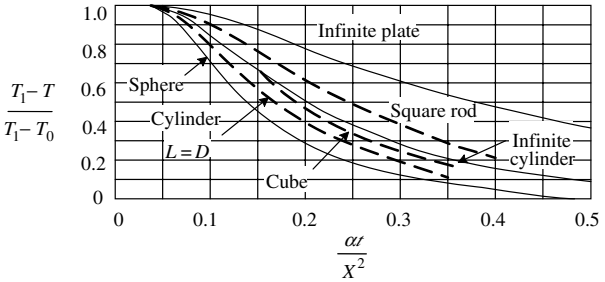

Fig. 5.8 Temperature at the center of different shapes versus time; X is the thickness, side dimension, or diameter; initial temperature is T_0, then the temperature of the outside surface is raised to T_1. [Reprinted by permission from H. Gröber and S. Erk, *Die Grundgesetze der Wärmeü bertragung*, Springer-Verlag, Berlin, 1933, Fig. 28, p. 58.]

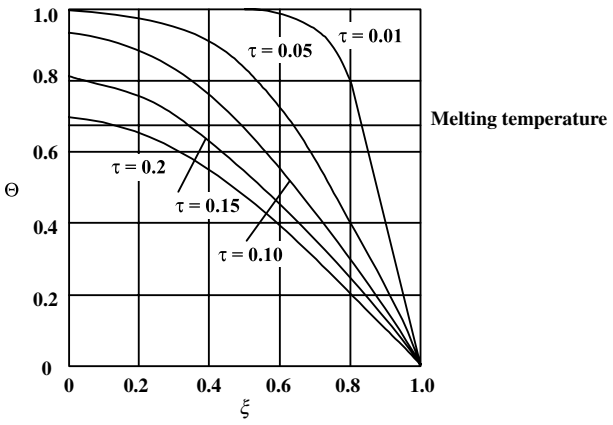

Fig. 5.9 Dimensionless temperature in a thin injection mold during solidification of HDPE. [Reprinted by permission from C. Gutfinger, E. Broyer, and Z. Tadmor, *Polym. Eng. Sci.*, **15**, 515 (1975).]

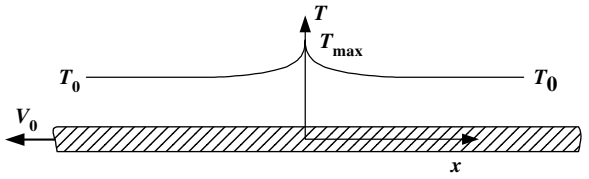

Fig. E5.5 Heating of a moving thin sheet with a plane heat source.

The energy equation for this problem reduces to:

$$\rho C_p V_0 \frac{dT}{dx} = k \frac{d^2T}{dx^2} - Q_v \tag{E5.5-1}$$

where Q_v is the heat exchanged with the surrounding per unit volume:

$$Q_v = \frac{hc}{A}[T(x) - T_0] \tag{E5.5-2}$$

where c and A are the perimeter and cross-sectional areas, respectively. Substituting Eq. E5.5-2 into Eq. E5.5-1 and using the "excess temperature" $T'(x) = T(x) - T_0$ instead of $T(x)$, we obtain

$$\frac{d^2T'}{dx^2} - \frac{V_0}{\alpha}\frac{dT'}{dx} - m^2T' = 0 \tag{E5.5-3}$$

where

$$m = \left(\frac{hc}{kA}\right)^{1/2} \tag{E5.5-4}$$

Equation E5.5-3 is to be solved subject to the boundary conditions $T'(\pm\infty) = 0$. Equation E5.5-3 is a linear second-order differential equation that can be conveniently solved by defining a differential operator $D^n = d^n/dx^n$, yielding

$$\left(D^2 - \frac{V_0}{\alpha}D - m^2\right)T' = 0 \tag{E5.5-5}$$

in which the differential operator behaves as though it were an algebraic polynomial. Since $T' \neq 0$, the expression in parentheses must equal zero, and solving for D, we get as roots:

$$D = \frac{V_0}{2\alpha} \pm \sqrt{m^2 + \left(\frac{V_0}{2\alpha}\right)^2} \tag{E5.5-6}$$

The temperature profile is then

$$T'(x) = A_1 \exp\left[\left(\frac{V_0}{2\alpha} + \sqrt{m^2 + \left(\frac{V_0}{2\alpha}\right)^2}\right)x\right] + B_1 \exp\left[\left(\frac{V_0}{2\alpha} - \sqrt{m^2 + \left(\frac{V_0}{2\alpha}\right)^2}\right)x\right] \tag{E5.5-7}$$

Since we cannot satisfy both boundary conditions except for the trivial case $T' = 0$, we split our solution into two regions $x \geq 0$ and $x \leq 0$, resulting in the following solutions:

$$T'(x) = B_1 \exp\left[-\left(\sqrt{m^2 + \left(\frac{V_0}{2\alpha}\right)^2} - \frac{V_0}{2\alpha}\right)x\right] \qquad x \geq 0 \tag{E5.5-8}$$

and

$$T'(x) = A_1 \exp\left[\left(\sqrt{m^2 + \left(\frac{V_0}{2\alpha}\right)^2} + \frac{V_0}{2\alpha}\right)x\right] \qquad x \leq 0 \tag{E5.5-9}$$

Now at $x = 0$ both equations should yield the same, yet unknown maximum temperature $T'_{\max}$; thus, we get

$$A_1 = B_1 = T'_{\max} = T'(0) \tag{E5.5-10}$$

The value of $T'_{\max}$ depends on the intensity of the heat source. Heat generated at the plane source is conducted in both the x and $-x$ directions. The fluxes q_1 and q_2, and in these respective directions are obtained from Eqs. E5.5-8 and E5.5-9:

$$q_1 = kT'_{\max}\left(\sqrt{m^2 + \left(\frac{V_0}{2\alpha}\right)^2} - \frac{V_0}{2\alpha}\right) \tag{E5.5-11}$$

$$q_2 = -kT'_{\max}\left(\sqrt{m^2 + \left(\frac{V_0}{2\alpha}\right)^2} + \frac{V_0}{2\alpha}\right) \tag{E5.5-12}$$

A heat balance at the interface requires

$$q = |q_1| + |q_2| \tag{E5.5-13}$$

Substituting Eqs. E5.5-11 and E5.5-12 into Eq. E5.5-13 and solving for $T'_{\max}$ gives

$$T'_{\max} = \frac{q}{2k\sqrt{m^2 + \left(\frac{V_0}{2\alpha}\right)^2}} \tag{E5.5-14}$$

Thus the maximum excess temperature is proportional to the intensity of the source, and it drops with increasing speed V_0, and increases in the thermal conductivity and the heat transfer coefficient. From Eqs. E5.5-8 and E5.5-9 we conclude that the temperature drops quickly in the positive x direction as a result of the convection ($V_0 < 0$) of the solid into the plane source, and slowly in the direction of motion. Again, in this chapter we encounter

exponentially dropping temperatures in solids with convection—a frequent situation in melting configurations.

5.5 SINTERING

When solid particles come in contact with each other at elevated temperatures, they tend to coalesce, thereby decreasing the total surface area. This process is called *sintering* (18). It is usually accompanied by a decrease in the total volume of the particulate bed. A decrease in surface area brings about a decrease in (surface) free energy; hence, the surface tension is the driving force for the coalescence process.

The sintering process proceeds in two distinct stages, first by developing interfaces and bridges between adjacent particles with little change in density, followed by a *densification* stage in which the interparticle cavities are eliminated (Fig. 5.10). It should be noted that sintering is a local phenomenon between adjacent particles involving viscous flow. The rate of the process is therefore greatly affected by the local temperature. Hence, along with the sintering process, we usually have to deal with the overall heat transfer problem within the particulate system, where previously discussed solutions are applicable, with the thermophysical properties replaced by ''effective'' values.

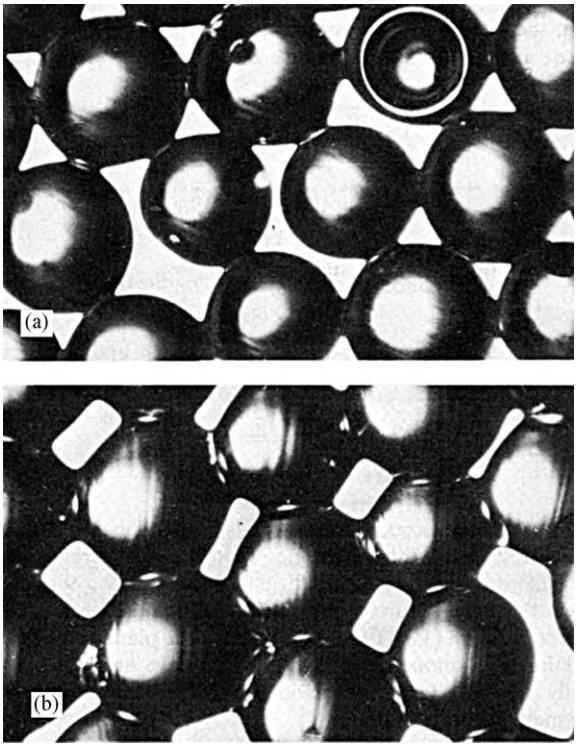

Fig. 5.10 A monolayer of 700 μm. diameter Polymethyl methacrylate (PMMA) beads during a sintering process at 203°C, × 50. (a) After 25 min; (b) after 55 min. [Reprinted by permission from M. Narkis, D. Cohen, and R. Kleinberger, ''Sintering Behavior and Characterization of PMMA Particles,'' Department of Chemical Engineering, Technion Israel Institute of Technology, Haifa.]

The processing of metallic and ceramic powders by sintering is an old and well-developed technological activity. In polymer processing, melting by a sintering process is practiced in areas such as rotational molding (19,20) and powder coating. Moreover, it provides the only practical way to process polytetrafluoroethylene, whose very high molecular weight precludes other common processing methods (21). Finally, a process of high-pressure compaction, followed by sintering, has been suggested for melting and shaping high-temperature polymers such as polyimides and aromatic polyesters, as well as for physical mixtures of preset composition distribution of more common polymers (22,23).

The model of viscous sintering was developed by Frenkel (24), who derived the following expression for the rate of coalescence of spherical adjacent particles:

$$\frac{x^2}{R} = \frac{2}{3}\frac{\Gamma}{\eta}t \tag{5.5-1}$$

subject to $x/R < 0.3$, where x is the neck radius (Fig. 5.11), R is the radius of the particles, Γ is the surface tension, and η is the viscosity. This expression was applied successfully to glass and ceramic materials, but for polymeric materials Kuczynski et al (18), working with polymethyl metacrylate (PMMA), found the experimental data to follow the following type of empirical equation:

$$\left(\frac{x^2}{R^{1.02}}\right)^p = F(T)t \tag{5.5-2}$$

where t is sintering time, and $F(T)$ is a function only of the temperature. For $p = 1$, Eq. 5.5-2 reduces to a Frenkel type of equation. Kuczynski et al. derived this equation theoretically by assuming the melt to be non-Newtonian and to follow the Power Law constitutive equation. The result is

$$\left(\frac{x^2}{R}\right)^{1/n} = \frac{t}{2n}\left(\frac{8n\Gamma}{m}\right)^{1/n} \tag{5.5-3}$$

where n and m are the Power Law model constants. Thus the parameter p in Eq. 5.5-2 acquires rheological meaning. For $n = 1$, Eq. 5.5-3 reduces to the Frenkel equation as corrected by Eshelby (25). Yet the flow field during the coalescence process is probably neither homogeneous nor isothermal; therefore, a complete analysis of the coalescence stage would first require a detailed analysis of the kinematics of the flow field. Thus, the theoretical analysis should preferably be carried out with a viscoelastic

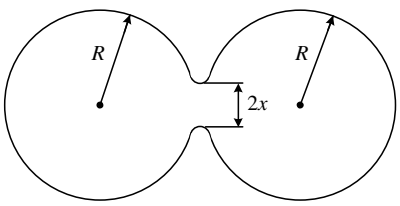

Fig. 5.11 Schematic view of the first stage in the sintering process.

constitutive equation, because viscoelastic effects, as suggested by Lonz (21), may play an important role in sintering of polymeric materials, and accounting for nonisothermal effects.

The coalescence stage is usually considered terminated when x/R reaches a value of 0.5. For the densification stage that follows, Frenkel (24) suggested the following expression:

$$\frac{r}{r_0} = 1 - \frac{\Gamma}{2\eta r_0} t \tag{5.5-4}$$

when r_0 is the initial radius of the approximately spherical cavity formed by the first stage, and r is the radius at time t.

As sintering proceeds and coalescence and densification occur, the overall heat conduction problem does not remain unaffected. Clearly, the effective thermophysical properties change, thereby influencing the overall temperature distribution and the local sintering problem as well.

5.6 CONDUCTION MELTING WITH FORCED MELT REMOVAL

In the preceding sections, we have discussed the physical mechanisms by which thermal energy can be supplied to a solid polymer, and have outlined some of the mathematical tools available for solving these problems. We have dealt with various aspects of ''conduction melting without melt removal,'' which is generally applicable to melting a semifinished or finished product, as well as to the solidification processes following shaping. We have noticed in most of the problems analyzed that heat fluxes and rates of melting diminish rapidly with time as the molten layer increases in thickness. It follows logically, then, that the rate of melting can be considerably increased by a *continuous removal of the molten layer formed*. This process, as Section 5.1 pointed out, not only leads to high rates of melting, but is the *essential element in creating a continuous steady source of polymer melt*, which in turn is the heart of the most important shaping methods of die forming, molding, calendaring, and coating, as well as for preparing the preshaped forms for the stretch shaping operations.

Removal of the melt, also discussed in Section 5.1, is made possible, in principle, by two mechanisms: drag-induced flow and pressure-induced flow (Fig. 5.4). In both cases, the molten layer must be sheared, leading to viscous dissipation. The latter provides an additional, important source of thermal energy for melting, the rate of which can be controlled externally either by the velocity of the moving boundary in drag-induced melt removal or the external force applied to squeeze the solid onto the hot surface, in pressure-induced melt removal.

In either of these cases we convert external mechanical energy into heat. This source of heat is not negligible; it may even be the dominant or sole source in the melting process, for example, in the case of ''autogenous'' screw extrusion.[3] Having two alternative sources of heat energy provides the processing design engineer with a great deal of flexibility.

3. This term is used for an extrusion operation where the barrel is heated for the start-up, but then heating is discontinued and the only source of heat is viscous dissipation.

Finally, the continuous removal of melt has the added benefit of not exposing polymer melts to high temperature surfaces or regions for long residence times.

From a mathematical point of view, problems of conduction melting with forced melt removal are far more complex than ordinary conduction melting, because they involve the simultaneous solution of the momentum and energy equations. Moreover, boundary conditions are often ill defined.

We will now analyze forced drag melt removal in some detail. This is the dominant melting mechanism in the SSE, and to a very large extent, in the injection molding machine as well. These, of course, are two very important devices for polymer processing forming operations. Chapter 6 discusses the flow in the single screw geometry from first principles, and Chapter 9 analyzes in detail the melting mechanism in single screw-based machines using the melting model presented in Section 5.7.

5.7 DRAG-INDUCED MELT REMOVAL

We consider an infinite slab of isotropic homogenous solid of width W, pressed against a moving hot plate (Fig. 5.12). A highly sheared, thin film of melt is formed between the

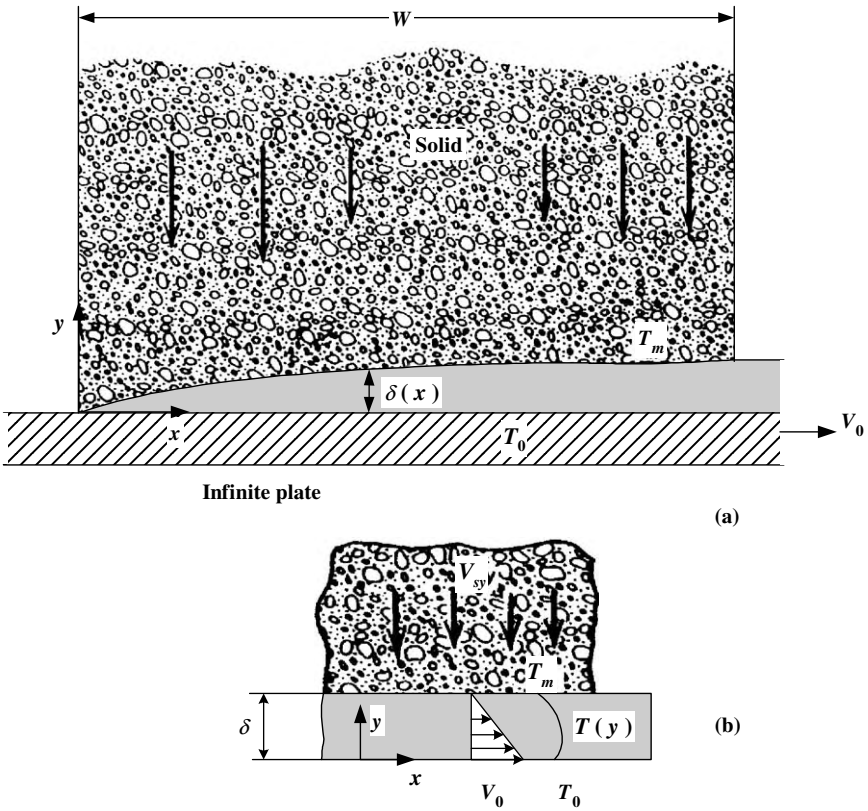

Fig. 5.12 (a) Schematic representation of a slab of polymer melting on a hot moving surface. (b) Enlarged view of a portion of the melt film.

solid and the plate, and this film is continuously removed. After a certain time, steady-state conditions evolve; that is, velocity and temperature profiles become time independent. The problem is two-dimensional, in that the temperature and velocity fields are functions of x and y only. No variations occur in the z direction, which is infinite. The thickness of the melt film is very small at $x = 0$, and it increases in the positive x direction, the shape of the melt film $\delta(x)$ being an a priori unknown function.

Heat is conducted from the hot plate, which is at a constant temperature T_0, to the solid–melt interface at $T = T_m$, assuming that the polymer is polycrystalline. As discussed in Section 5.1, amorphous polymers at T_g do not change abruptly from brittle solids to viscous liquids. Thus the choice for T_m is not obvious. One can pretend that the transition is sharp and set an arbitrary level of temperature (larger than T_g) at which flow begins to occur. Alternatively, as suggested recently by Sundstrom and Lo (26), the glass transition temperature can be used together with the WLF equation to select an appropriate melting point.

We are seeking a solution for the rate of melting and the temperature distribution of the emerging melt. Clearly, these variables will be functions of the *physical properties* of the solid, the *plate temperature* and velocity, and the *width of the solid* slab.

The drag-removal melting mechanism was discovered and mathematically modeled by Tadmor (27) in connection to melting in SSEs (see Section 9.3). It was further refined, experimentally, verified, and formulated as a self-contained computer package by Tadmor et al. (28–31). Later Vermeulen et al. (32), and Sundstrom and Lo (26) and Sundstrom and Young (33) analyzed the problem both experimentally and theoretically; Mount (34) measured experimental rates of melting, and Pearson (35) analyzed the theoretical problem mathematically in detail, as shown in Fig. 5.12. In this section we follow Pearson's discussion.

In trying to analyze the detailed mechanism of this melting configuration, we must first consider the nature of the solid. For a perfectly rigid, incompressible body moving toward the interface without rotation, the rate of melting at the interface must be independent of the coordinate x, because the bulk velocity of the solid will be uniform across x. Hence, $\delta(x)$ and $P(x)$, and the velocity and temperature fields in the film *must* assume values that will satisfy this requirement, as well as the equations of motion and energy, with the appropriate boundary conditions. But in highly sheared thin films of very viscous polymers formed under a relatively soft deformable bed of particulate solids, a constant pressure assumption in the film is more appropriate. This, in turn, implies that, at steady-state conditions, the *rate of melting* may generally be a *function* of x, although this variation may be small. A *variable* melting rate therefore implies, that the solid either *deforms* or *rotates* or does both.

Solid polymers, in particular, in the form of a bed of compressed pellets or powder as encountered in polymer processing, can be considered deformable. The melt formed at the interface penetrates some of the voids between the particulate solids forming the bed, enabling sliding and rearrangement in the neighborhood of the interface. Through such a mechanism, it is easy to visualize the continuously deforming solid concept. Thus, the physical situation in this case would be one of a slowly deformable solid pressed against the moving hot plate.

The solid interface has a small velocity in the negative y direction that may slowly vary with x. Yet the solid is *rigid enough* to sustain the shear stresses in the film and to prohibit the development of an x-direction interface velocity. We are now in a position to state the

simplifying assumptions to the problem and specify the governing differential equations. The following assumptions are made:

1. Constant thermophysical properties
2. Incompressible fluid
3. No slip at the wall
4. Power Law (or Newtonian) fluid with temperature-dependent viscosity:

$$m = m_0 e^{-a(T-T_m)} \tag{5.7-1}$$

5. Steady state conditions
6. Negligible gravitational forces
7. Laminar flow prevails throughout
8. The film thickness is much smaller than its width $\delta/W \ll 1$

These, together with the small Reynolds number in the film, justifies the use of the lubrication approximation. Moreover, the same considerations lead us to neglect exit effects (at $x = W$), and precise entrance conditions (at $x = 0$) need not be specified.

The equations of continuity and motion, respectively, reduce to

$$\frac{\partial v_x}{\partial x} + \frac{\partial v_y}{\partial y} = 0 \tag{5.7-2}$$

and

$$\frac{\partial P}{\partial x} = \frac{\partial \tau_{yx}}{\partial y} \tag{5.7-3}$$

Since we assume a pure drag flow in the film, Eq. 5.7-3 further reduces to

$$\frac{\partial \tau_{yx}}{\partial y} = 0 \tag{5.7-4}$$

Expressing the shear stress in terms of the local velocity gradient, Eq. 5.7-4 becomes

$$\frac{\partial}{\partial y}\left[e^{-a(T-T_m)}\left(-\frac{\partial v_x}{\partial y}\right)^n\right] = 0 \tag{5.7-5}$$

Equation 5.7-5 can be integrated with respect to y to give

$$-\left(\frac{\partial v_x}{\partial y}\right) = C_1 e^{[a(T-T_m)/n]} \tag{5.7-6}$$

Thereby, if $a = 0$ (i.e., temperature-independent viscosity), the velocity profile is linear for both Newtonian and Power Law fluids. If, however, $a \neq 0$, the local velocity profile

becomes a function of the temperature. Since temperature varies sharply over y, we expect significant nonlinearity of the profile in the y direction. Moreover, because of convection, T is also a (weaker) function of x, introducing a corresponding (weak) x dependence of the velocity profile. Hence, the equations of motion and energy must be solved simultaneously. The latter reduces to

$$\rho_m C_m \left(v_x \frac{\partial T}{\partial x} + v_y \frac{\partial T}{\partial y} \right) = k_m \frac{\partial^2 T}{\partial y^2} - \tau_{xy} \frac{\partial v_x}{\partial y} \tag{5.7-7}$$

where ρ_m, C_m, and k_m are the thermophysical properties of the polymer melt, with heat conduction in the x direction assumed to be much smaller than conduction in the y direction, and further assuming that the only significant contribution to viscous dissipation is that originating from the τ_{yx} component of the stress tensor.

Next we specify the boundary conditions in the film. At the solid boundary we have:

$$T(0) = T_0, \qquad v_x(0) = V_0, \qquad v_y(0) = 0 \tag{5.7-8}$$

and at the solid–melt interface we have:

$$T(\delta) = T_m, \qquad v_x(\delta) = 0 \tag{5.7-9}$$

The velocity $v_y(\delta)$ at any position x is determined by the rate of melting at the interface, to be obtained from the following heat balance:

$$\underset{\substack{\text{Rate of heat conducted}\\ \text{intothe interface per unit}\\ \text{interface area}}}{k_m \left(-\frac{\partial T}{\partial y} \right)_{y=\delta}} = \underset{\substack{\text{Rate of melting at the}\\ \text{interface per unit interface}\\ \text{area timesthe heat of fusion}}}{\rho_m [-v_y(\delta)]\lambda} + \underset{\substack{\text{Rate of heat conducted}\\ \text{out of the interface per}\\ \text{unit interface area}}}{k_s \left(-\frac{\partial T_s}{\partial y} \right)_{y=\delta}} \tag{5.7-10}$$

where λ is the heat of fusion, and k_s and T_s are the thermal conductivity and temperature, respectively, of the solid. The term on the left-hand side is the rate of heat conducted from the hot film into the interface.

For melting to take place, $\partial T/\partial y < 0$. This term is therefore positive and provides the heat source for melting, which as we see on the right-hand side, is used for two purposes: to heat the polymer to the melting point at the interface where $T = T_m$ (second term) and to melt the polymer at the interface (first term).

The last term on the right-hand side can be obtained by solving the temperature profile in the solid bed. Consider a small, x-direction portion of the film and solid [Fig. 5.12(b)]. We assume the solid occupies the region $y > \delta$ (where δ is the local film thickness) and moves into the interface with constant velocity v_{sy}. The problem thus reduces to a one-dimensional steady heat-conduction problem with convection. In the solid, a steady, exponentially dropping temperature profile develops. The problem is similar to that in Section 5.4. The equation of energy reduces to

$$\rho_s C_s v_{sy} \frac{\partial T_s}{\partial y} = k_s \frac{\partial^2 T_s}{\partial y^2} \tag{5.7-11}$$

where ρ_s, C_s, and k_s are the thermophysical properties of the solid polymer. Equation 5.7-11 can be easily solved with the boundary conditions $T_s(\delta) = T_m$ and $T_s(\infty) = T_{s0}$, to give the following temperature profile:

$$T = T_{s0} + (T_m - T_{s0}) \exp\left[\frac{v_{sy}(y - \delta)}{\alpha_s}\right] \tag{5.7-12}$$

The velocity $v_{sy} < 0$, and hence Eq. 5.7-12, satisfies both boundary conditions. The rate of heat conduction out of the interface, noting that $v_{sy}\rho_s = v_y(\delta)_y\rho_m$, is

$$-k_s\left(\frac{\partial T}{\partial y}\right)_{y=\delta} = -(T_m - T_{s0})v_y(\delta)\rho_m C_s \tag{5.7-13}$$

Thus Eq. 5.7-10 can now be written as

$$k_m\left(\frac{\partial T}{\partial y}\right)_{y=\delta} = \rho_m v_y(\delta)\lambda^* \tag{5.7-14}$$

where

$$\lambda^* = \lambda + C_s(T_m - T_{s0}) \tag{5.7-15}$$

Thus λ^* is the total heat energy required to bring a *solid* from an initial temperature T_{s0} to T_m and to *melt* it at that temperature. Sundstrom and Young (33) solved this set of equations numerically after converting the partial differential equations into ordinary differential equations by similarity techniques. Pearson (35) used the same technique to obtain a number of useful solutions to simplified cases. He also used dimensionless variables, which aid in the physical interpretation of the results, as shown below:

$$\Theta = \frac{T - T_m}{T_0 - T_m} \tag{5.7-16}$$

$$\xi = \frac{x}{W} \qquad \text{and} \qquad \eta = \frac{y}{\delta} \tag{5.7-17}$$

$$u_x = \frac{v_x}{V_0} \qquad \text{and} \qquad u_y = \frac{v_y}{V_0(\delta_0/W)} \tag{5.7-18}$$

where the meaning of δ_0 will be clarified below.

We first rewrite the boundary conditions

$$\Theta(0) = 1, \qquad u_x(0) = 1, \qquad u_y(0) = 0 \tag{5.7-19}$$

$$\Theta(1) = 0, \qquad u_x(1) = 0 \tag{5.7-20}$$

The melting condition at the interface (Eq. 5.7-14) reduces to

$$\frac{k_m(T_0 - T_m)W}{\lambda^*\rho_m V_0 \delta_0^2}\left(\frac{\partial \Theta}{\partial \eta}\right)_{\eta=1} = \frac{\delta}{\delta_0}u_y(1) \tag{5.7-21}$$

This relationship provides us with a reasonable choice of δ_0. Since this boundary condition determines the physical process, the dimensionless group $k_m(T_0 - T_m)W/\lambda^*\rho_m V_0\delta_0^2$ should be of the order of 1. Hence, we can *choose* δ_0 as

$$\delta_0 = \left(\frac{k_m(T_0 - T_m)W}{\lambda^*\rho_m V_0}\right)^{1/2} \tag{5.7-22}$$

As we shall see later, δ_0 is not merely an arbitrary scaling (normalizing) factor; by the choice we made it turns out to be of the order of the film thickness, provided viscous dissipation or convection are not too significant to the process.

We now can rewrite the transport equation in dimensionless form as follows. The continuity equation is

$$\frac{\partial u_x}{\partial \xi} - \eta\frac{\dot{\delta}}{\delta}\frac{\partial u_x}{\partial \eta} + \frac{\delta_0}{\delta}\frac{\partial u_y}{\partial \eta} = 0 \tag{5.7-23}$$

where $\dot{\delta} = d\delta/d\xi$.

Details of the derivation of Eq. 5.7-23 are as follows. Substituting u_x and u_y from Eq. 5.7-18 into the equation of continuity results in

$$V_0\frac{\partial u_x}{\partial x} + \frac{V_0\delta_0}{W}\frac{\partial u_y}{\partial y} = 0$$

Next we rewrite the partial differentials in terms of the new variables η and ξ. We recall that $u_x(\xi,\eta), u_y(\eta), \xi = F_1(x)$, and $\eta = F_2(x,y)$. The x dependence in η is due to $\delta(x)$. Hence, we can write

$$\begin{aligned}\frac{\partial u_x}{\partial x} &= \frac{\partial u_x}{\partial \xi}\frac{\partial \xi}{\partial x} + \frac{\partial u_x}{\partial \eta}\frac{\partial \eta}{\partial x} = \frac{1}{W}\frac{\partial u_x}{\partial \xi} - \frac{y}{\delta^2}\frac{\partial \delta}{\partial x}\frac{\partial u_x}{\partial \eta} \\ &= \frac{1}{W}\frac{\partial u_x}{\partial \xi} - \frac{\eta}{W}\frac{\dot{\delta}}{\delta}\frac{\partial u_x}{\partial \eta}\end{aligned}$$

Similarly, we obtain

$$\frac{\partial u_y}{\partial y} = \frac{\partial u_y}{\partial \xi}\frac{\partial \xi}{\partial y} + \frac{\partial u_y}{\partial \eta}\frac{\partial \eta}{\partial y} = \frac{1}{\delta}\frac{\partial u_y}{\partial \eta}$$

The dimensionless form of the equation of motion is

$$\frac{\partial}{\partial \eta}\left[e^{b\Theta}\left(-\frac{\partial u_x}{\partial \eta}\right)^n\right] = 0 \tag{5.7-24}$$

where

$$b = -a(T_0 - T_m) \tag{5.7-25}$$

Finally the equation of energy using the definition of δ_0 becomes

$$M^{-1}\left[u_x\frac{\partial\Theta}{\partial\xi}-u_x\frac{\dot{\delta}}{\delta}\eta\frac{\partial\Theta}{\partial\eta}+u_y\frac{\delta_0}{\delta}\frac{\partial\Theta}{\partial\eta}\right]$$
$$=\left(\frac{\delta_0}{\delta}\right)^2\frac{\partial^2\Theta}{\partial\eta^2}+\mathrm{Br}\left(\frac{\delta_0}{\delta}\right)^{n+1}e^{b\Theta}\left(-\frac{\partial u_x}{\partial\eta}\right)^{n+1} \tag{5.7-26}$$

where

$$M=\frac{\lambda^*}{C_m(T_0-T_m)} \tag{5.7-27}$$

and

$$\mathrm{Br}=\frac{m_0V_0^{(3n+1)/2}\rho_m^{(n-1)/2}\lambda^*(n-1)/2}{(T_0-T_m)^{(n+1)/2}k_m^{(n+1)/2}W^{(n-1)/2}} \tag{5.7-28}$$

In these equations, Br is a modified Brinkman number, which is a measure of the extent to which viscous heating is important, and M measures the ratio of heat energy needed to melt the polymer, as compared to that needed to heat the melt to T_0. If the latter is small, M will be large and the convection terms in the energy equation can be neglected. The dimensionless parameter b measures the significance of the temperature dependence of the viscosity over the temperature range considered (flow activation energy).

Achieving a complete solution of the set of equations above is difficult, as pointed out earlier. In addition to the numerical solution (33), Pearson (35) proposed a heuristic approach. Insight into the nature of melting with drag-forced removal can be obtained, however, by considering some special cases that lead to analytical, closed-form solutions. These simplified cases per se represent very useful solutions to the modeling of processing methods.

Newtonian Fluid with Temperature-Independent Viscosity and Negligible Convection

For a Newtonian fluid close to isothermal conditions (i.e., $n=1$ and $b\ll 1$), and with convection neglected (i.e., $M\gg 1$), the equation of motion becomes

$$\frac{\partial^2 u_x}{\partial\eta^2}=0 \tag{5.7-29}$$

which, for the boundary conditions stated in Eqs. 5.7-19 and 5.7-20 has the solution

$$u_x=1-\eta \tag{5.7-30}$$

The equation of energy, which for this case can be solved independently, reduces to

$$\frac{\partial^2\Theta}{\partial\eta^2}+\mathrm{Br}\left(-\frac{\partial u_x}{\partial\eta}\right)^2=0 \tag{5.7-31}$$

Substituting Eq. 5.7-30 into Eq. 5.7-31, followed by integration, yields the temperature profile

$$\Theta = 1 - \eta + \frac{\mathrm{Br}}{2}\eta(1-\eta) \tag{5.7-32}$$

The mean temperature $\bar{\Theta}$ is obtained from Eq. 5.7-32 as follows:

$$\bar{\Theta} = \frac{\int_0^1 u_x \Theta \, d\eta}{\int_0^1 u_x \, d\eta} = \frac{2}{3} + \frac{\mathrm{Br}}{12} \tag{5.7-33}$$

Now we can solve Eq. 5.7-21 for u_y (1) by substituting from Eq. 5.7-32 $(\partial\Theta/\partial\eta)_{n=1} = -(1 + \mathrm{Br}/2)$ to obtain

$$u_y(1) = -\frac{\delta_0}{\delta}\left(1 + \frac{\mathrm{Br}}{2}\right) \tag{5.7-34}$$

Finally, we turn to the equation of continuity and integrate it over η, after substituting $\partial u_x/\partial\eta = -1$ from Eq. 5.7-30 and noting that $\partial u_x/\partial\xi = 0$, to obtain

$$u_y(1) = -\frac{1}{2}\frac{\dot{\delta}}{\delta_0} \tag{5.7-35}$$

Combining Eqs. 5.7-34 and 5.7-35 subsequent to integration yields the film profile $\delta(\xi)$

$$\delta = \delta_0\sqrt{(4 + 2\mathrm{Br})\xi} \tag{5.7-36}$$

We have obtained the important result that, with convection neglected, the film thickness is proportional to the square root of the distance. The rate of melting (per unit width) is now given by

$$w_L(x) = \rho_m V_0 \delta \int_0^1 u_x \, d\eta = \frac{V_0\delta}{2}\rho_m \tag{5.7-37}$$

By substituting Eq. 5.7-36 into 5.7-37 with $\xi = 1$ and δ_0 from Eq. 5.7-22, we obtain

$$\begin{aligned} w_L &= \left[V_0^2\delta_0^2\rho_m^2\left(1 + \frac{\mathrm{Br}}{2}\right)\right]^{1/2} = \left[\frac{V_0\rho_m k_m(T_0 - T_m)}{\lambda^*}\left(1 + \frac{\mathrm{Br}}{2}\right)W\right]^{1/2} \\ &= \left[\frac{V_0\rho_m\left[k_m(T_0 - T_m) + \mu V_0^2/2\right]W}{\lambda^*}\right]^{1/2} \end{aligned} \tag{5.7-38}$$

The physical meaning of the various terms now becomes evident. The numerator in the square bracket in the last expression contains the sum of heat conduction and viscous dissipation terms. The denominator is the heat energy needed to heat the solid from T_{s0} to melt at T_m. The rate of melting also increases proportionally with the square root of the

plate velocity and slab width. Yet an increase in plate velocity also increases the viscous dissipation.

In this expression we have neglected convection in the film. Tadmor et al. (28) and Tadmor and Klein (29) made an approximate accounting for convection by replacing λ^* with an expression that includes the heat needed to bring the melt from T_m to the mean melt temperature

$$\lambda^{**} = \lambda + C_s(T_m - T_{s0}) + C_m(T_0 - T_m)\bar{\Theta} \tag{5.7-39}$$

Furthermore, by carrying out the mental exercise of ''removing'' the newly melted material from the interface, ''carrying'' it to $\xi = 0$, and allowing it to flow into the film at that point, the film thickness will stay constant and the resulting effect will be a reduction of w_L in Eq. 5.7-38 by a factor of $\sqrt{2}$.

Power Law Model Fluid with Temperature Dependent Viscosity

Both shear thinning and temperature dependence of viscosity strongly affect the melting rate. Their effect on the rate of melting can be estimated by considering a case in which convection is neglected and viscous dissipation is low enough to permit the assumption that the viscosity variation across the film is determined by a linear temperature profile:

$$\Theta = 1 - \eta \tag{5.7-40}$$

The equation of motion (Eq. 5.7-24) reduces to

$$\frac{\partial}{\partial \eta}\left[e^{b[1-\eta]}\left(-\frac{\partial u_x}{\partial \eta}\right)^n\right] = 0 \tag{5.7-41}$$

Equation 5.7-41 can be solved for the local velocity profile $u_x(\eta)$

$$u_x = \frac{e^{b'\eta} - e^{b'}}{1 - e^{b'}} \tag{5.7-42}$$

where

$$b' = \frac{b}{n} = -\frac{a(T_0 - T_m)}{n} \tag{5.7-43}$$

Clearly, b' is a dimensionless number that takes into account both the temperature and shear rate viscosity dependence.

The equation of energy (Eq. 5.7-26), reduces in this case to

$$\frac{\partial^2 \Theta}{\partial \eta^2} + \mathrm{Br}\left(\frac{\delta_0}{\delta}\right)^{n-1} e^{b(1-\eta)}\left(-\frac{\partial u_x}{\partial \eta}\right)^{n+1} = 0 \tag{5.7-44}$$

Substituting Eq. 5.7-42 into Eq. 5.7-44, followed by integration, yields

$$\Theta = (1-\eta) + \mathrm{Br}\left(\frac{\delta_0}{\delta}\right)^{n-1}\left(\frac{b'}{1-e^{-b'}}\right)^{n+1}\left(\frac{e^{-b'}}{b'^2}\right)\left[1 - e^{b'\eta} - \eta\left(1-e^{b'}\right)\right] \tag{5.7-45}$$

As in the Newtonian case, we solve Eq. 5.7-21 for $u_y(1)$, after obtaining $(\partial\Theta/\partial\eta)_{\eta=1}$ from Eq. 5.7-45

$$u_y(1) = -\left(\frac{\delta_0}{\delta}\right)\left[1 + \mathrm{Br}\left(\frac{\delta_0}{\delta}\right)^{n-1}\left(\frac{b'}{1-e^{-b'}}\right)^{n+1}\left(\frac{b'-1+e^{-b'}}{b'^2}\right)\right] \tag{5.7-46}$$

Finally, the equation of continuity (Eq. 5.7-23), with $\partial u_x/\partial\xi = 0$ and subsequent to substituting $\partial u_x/\partial\eta$ from Eq. 5.7-42, results in

$$-\eta\left(\frac{\dot{\delta}}{\delta_0}\right)\left(\frac{b'e^{b'\eta}}{1-e^{b'}}\right) + \frac{\partial u_y}{\partial\eta} = 0 \tag{5.7-47}$$

which is integrated to give

$$u_y(1) = \frac{\dot{\delta}}{\delta_0}\left[\frac{1}{b'(1-e^{b'})}\right]\left[e^{b'}(b'-1)+1\right] \tag{5.7-48}$$

Combining Eqs. 5.7-46 and 5.7-48 results in a differential equation for δ

$$\delta\frac{d\delta}{d\xi} = \frac{-\delta_0^2\left[1 + \mathrm{Br}\left(\frac{\delta_0}{\delta}\right)^{n-1}\left(\frac{b'}{1-e^{-b'}}\right)^{n+1}\left(\frac{b'-1+e^{-b'}}{b'^2}\right)\right]}{\frac{e^{b'}(b'-1)+1}{b'(1-e^{b'})}} \tag{5.7-49}$$

An approximate solution of Eq. 5.7-49 can be obtained if a mean δ value is assumed in the term $(\delta_0/\delta)^{n-1}$. This is a weak dependence of the viscous dissipation term on δ. The resulting melt film profile is

$$\delta = \delta_0\left\{\frac{4\left[1 + \mathrm{Br}\left(\frac{\delta_0}{\bar{\delta}}\right)^{n-1}\left(\frac{b'}{1-e^{-b'}}\right)^{n+1}\left(\frac{b'-1+e^{-b'}}{b'^2}\right)\right]\xi}{U_2}\right\}^{1/2} \tag{5.7-50}$$

where

$$U_2 = 2\frac{1-b'-e^{-b'}}{b'(e^{-b'}-1)} \tag{5.7-51}$$

By substituting the expressions of δ_0 and Br from Eqs. 5.7-22 and 5.7-28, respectively, Eq. 5.7-50 can be written as

$$\delta = \left\{ \frac{2[2k_m(T_0 - T_m) + U_1]x}{U_2 \rho_m V_0 \lambda^*} \right\}^{1/2} \tag{5.7-52}$$

where

$$U_1 = \frac{2m_0 V_0^{n+1}}{(\bar{\delta})^{n-1}} \left(\frac{b'}{1 - e^{-b'}} \right)^{n+1} \left(\frac{b' - 1 + e^{-b'}}{b'^2} \right) \tag{5.7-53}$$

The rate of melting (per unit width) is given by

$$w_L(x) = \rho_m V_0 \delta \int_0^1 u_x \, d\eta = \frac{V_0 \delta \rho_m}{2} U_2 \tag{5.7-54}$$

And substituting δ from Eq. 5.7-52 into Eq. 5.7-54 gives

$$w_L(x) = \left\{ \frac{\rho_m V_0 U_2 [k_m(T_0 - T_m) + U_1/2]x}{\lambda^*} \right\}^{1/2} \tag{5.7-55}$$

Thus the physical significance of U_2 and U_1 becomes evident. The former reflects the reduction ($U_2 < 1$) of the rate of melt removal of the film by drag flow as a result of temperature dependence and shear thinning of the viscosity, whereas $U_1/2$ is the rate of viscous dissipation (per unit width) in the melt film. The relative significance of conduction and dissipation for melting is obtained by comparing the two terms in the square Brackets in Eq. 5.7-55.

If convection is to be accounted for by the same approximate method as described in the previous Newtonian case, then λ^* in Eq. 5.7-55 is replaced by λ^{**}, which is given in Eq. 5.7-39, and $w_L(x)$ given in Eq. 5.7-55 is reduced by a factor of $\sqrt{2}$. Finally, the mean temperature of the film

$$\bar{\Theta} \equiv \frac{\int_0^1 u_x \Theta \, d\eta}{\int_0^1 u_x \, d\eta} \tag{5.7-56}$$

is obtained by substituting Eqs. 5.7-40 and 5.7-42 into Eq. 5.7-56

$$\bar{\Theta} = \frac{b'/2 + e^{-b'}(1 + 1/b') - 1/b'}{b' + e^{-b'} - 1} \tag{5.7-57}$$

This is an approximate expression because, for the sake of simplicity, a linear temperature profile was used rather than Eq. 5.7-45. The preceding expressions were applied to the solution of the melting problem in screw extruders (28,29). This is discussed in Chapter 9.

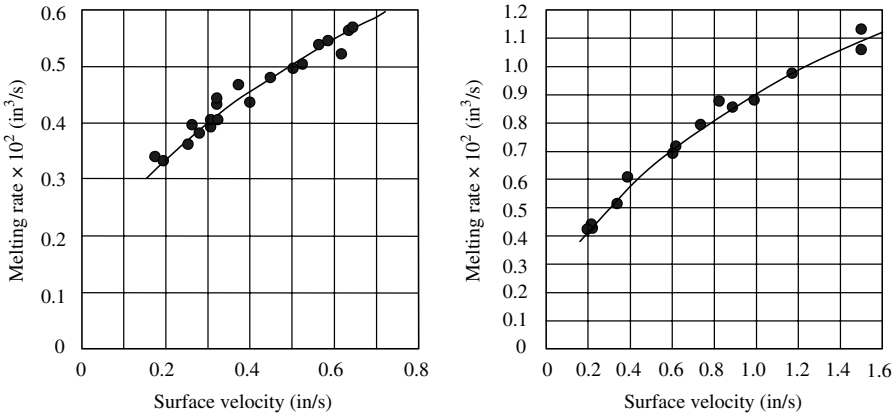

Fig. E5.6 Rate of melting of a 2 × 2-in block of HDPE on a hot rotating drum. (a) Drum temperature at 154°C. (b) Drum temperature at 168°C. Rate of melting measured in volume of displaced solid. [Reprinted by permission from D. H. Sundstrom and C. Young, "Melting Rates of Crystalline Polymers under Shear Conditions," *Polym. Eng. Sci*., **12**, 59 (1972).]

Example 5.6 Drag-induced Melt Removal Melting The rate of melting of a 2 × 2 in. block of solid HDPE at room temperature of 25°C on a hot rotating drum was measured by Sundstrom and Young (33). Their results appear in Fig. E5.6. (a) Analyze the effects of drum speed and temperature in light of the previously derived theoretical models. (b) Calculate the rate of melting at a drum speed of 1 in/s on a 168°C drum, using a Newtonian model and compare it to the experimental value. (c) Repeat step (b) with a Power Law model with a linear temperature profile in the melt film.

The rheological properties of the HDPE used in the experiments follow a Power Law model (33)

$$\eta = 4.0334 \times 10^3 e^{-0.010872(T-127)} \dot{\gamma}^{-0.547}$$

where η is the non-Newtonian viscosity (N·s/m^2), T is the temperature (°C), and $\dot{\gamma}$ is the shear rate s^{-1}. The Power Law exponent is $n = 0.453$. The melting point (33) is 127°C. The heat of fusion is 218 kJ/kg. The specific heat of the solid polymer is 2.3 kJ/kg ·°C, and that of the melt (28) is 2.512 kJ/kg ·°C. The thermal conductivity of HDPE melt is a function of temperature (36)

$$k = 0.0573 + 0.0010467T$$

where k is in W/m ·°C and T is the temperature (°C). Finally, the density of the solid polymer is 955 kg/m^3 and that of the melt (28) is 776 kg/m^3.

Solution

(a) The first step is to evaluate the relative significance of heat conduction and viscous dissipation. This is provided by the Brinkman number in Eq. 5.7-28, which for a Newtonian liquid, reduces to

$$\mathrm{Br} = \frac{\mu V_0^2}{k_m(T_0 - T_m)}$$

An estimate of the melt viscosity can be obtained from the Power Law expression given earlier, assuming a shear rate of $50\,s^{-1}$ and taking a mean temperature of $(168 + 127)/2 = 147.5°C$. (We will check later whether these assumptions are acceptable.) This yields

$$\mu = (4.0334 \times 10^3)e^{-0.010872(147.5-127)}(50)^{-0.547}$$
$$= 379.8\,N \cdot s/m^2$$

The tangential velocity of the drum selected is 1 in/s, or $V_0 = 0.0254 m/s$, and the thermal conductivity at the mean temperature is 0.212 W/m°C. Thus

$$Br = \frac{(379.8)(0.0254)^2}{(0.212)(168 - 127)} = 0.0282$$

Clearly, viscous dissipation is not significant in the experimental range given for the 168°C drum temperature experiments. Neither is it significant for the lower drum temperature experiments, which were conducted at lower drum speeds. It follows from the theoretical models (Eqs. 5.7-38 and 5.7-55) that the rate of melting in this case is proportional to the square root of drum speed and the temperature difference $(T_0 - T_m)$

$$w_L \propto \sqrt{V_0(T_0 - T_m)}$$

It is easy to verify that the curves in Fig. E5.6 follow quite well the predicted increase in rate of melting with drum speed. For example, the predicted rate of melting at 1.6 in/s from the corresponding value at 0.2 in/s is $0.4\sqrt{1.6/0.2} = 1.13\ in^3/s$, which is very close to the measured value. Similarly, selecting a fixed drum speed of 0.5 in/s, the measured rate of melting at 154°C is 0.5 in^3/s. The predicted value at 168°C is $0.5\sqrt{(168 - 127)/(154 - 127)} = 0.616\,in^3/s$, which once again is very close to the measured value.

(b) The rate of melting is evaluated from Eq. 5.7-38. First, however, the viscosity calculation is reexamined. This is done by calculating the film thickness from Eqs. 5.7-22 and 5.7-36. The former gives δ_0 with $W = 0.0508$ m and with λ^* calculated from Eq. 5.7-15

$$\lambda^* = 218 \times 10^3 + 2.3 \times 10^3(127 - 25) = 452.6 \times 10^3\ J/kg$$

Thus

$$\delta_0 = \left[\frac{(0.212)(168 - 127)(0.0508)}{(452.6 \times 10^3)(776)(0.0254)}\right]^{1/2} = 2.225 \times 10^{-4} m$$

and the maximum film thickness at $\xi = 1$ from Eq. 5.7-36 is

$$\delta_{max} = 2.225 \times 10^{-4}\sqrt{(4) + (2)(0.0282)} = 4.481 \times 10^{-4}\ m$$

The mean film thickness is 3.353×10^{-4} m, and the mean shear rate is $0.0254/3.353 \times 10^{-4} = 76\,s^{-1}$. The mean temperature is obtained from Eq. 5.7-33

$$\bar{\Theta} = \frac{2}{3} + \frac{0.0282}{12} = 0.669$$

Hence, $\bar{T} = 0.669(168 - 127) + 127 = 154.4$. Repeating the calculations with the viscosity evaluated at 76 s^{-1} and 154°C temperature, and with thermal conductivity of 0.218 W/m·°C, results in a viscosity of 281 $N \cdot s/m^2$, $Br = 0.0203$, $\delta_0 = 2.256 \times 10^{-4}$ m, a mean film thickness of 3.495×10^{-4} m, a mean shear rate of 73 s^{-1}, and a mean temperature of 154°C.

Using these values, the rate of melting is calculated from Eq. 5.7-38

$$w_L = \left[(0.0254)^2\left(2.256 \times 10^{-4}\right)^2(776)^2(1 + 0.0203/2)\right]^{1/2}$$
$$= 4.469 \times 10^{-3}\,\text{kg/m} \cdot \text{s}$$

The rate of melting for the whole block is $(4.469 \times 10^{-3})(0.0508) = 2.27 \times 10^{-4}$ kg/s, which is equivalent to 0.0145 in^3/s (note that the volume measured by Sundstrom and Young (33) is the displaced solid). Comparing this result with the measured value of 0.009 in^3/s indicates that the Newtonian model overestimates the rate of melting by about 60%. In the model used, the effect of convection in the film was neglected. By accounting for convection as discussed earlier, the rate of melting is given by

$$w_L = \left[\frac{V_0\rho_m\left[k_m(T_0 - T_m) + \mu V_0^2/2\right]W}{2\left[\lambda^* + C_m(T_0 - T_m)\bar{\Theta}\right]}\right]$$
$$= \left\{\frac{(0.0154)(776)\left[(0.218)(168 - 127) + (281)(0.0254)^2/2\right](0.0508)}{2[(452.6 \times 10^3) + (2.512 \times 10^3)(168 - 127)(0.669)]}\right\}^{1/2}$$
$$= 2.945 \times 10^{-3}\,\text{Kg/m} \cdot \text{s}$$

which results in a total rate of melting of 0.00956 in^3/s. This is only 6% above the measured value.

(c) To calculate the rate of melting from Eq. 5.7-55 we first calculate b',U_1, and U_2 as follows:

$$b' = -\frac{(0.010872)(168 - 127)}{(0.453)} = -0.984$$

From Eq. 5.7.51, U_2 is obtained

$$U_2 = (2)\frac{(-0.984) - (1) + e^{0.984}}{(-0.984)(1 - e^{0.984})} = 0.839$$

which indicates that the reduction in drag removal due to temperature dependence of viscosity is 16%. Finally, U_1 is obtained from Eq. 5.7-53 using the previously estimated mean film thickness

$$U_1 = \frac{(2)(4.0334 \times 10^3)(0.0254)^{1.453}}{(3.495 \times 10^{-4})^{-0.547}}\left(\frac{0.984}{e^{0.984} - 1}\right)^{1.453}\left(\frac{(-0.984) - 1 + e^{0.984}}{(-0.984)^2}\right)$$
$$= 0.1644\,\text{J/s} \cdot \text{m}$$

Substituting these values into Eq. 5.7-55, with λ^* replaced by λ ** and a factor of 2 in the denominator to account for convection, and with $\bar{\Theta}$ from Eq. 5.7-57, gives

$$w_L = \left\{\frac{(0.0254)(776)(0.839)[(0.218)(168 - 127) + (0.1644)/(2)]0.0508}{(2)[(452.6 \times 10^3) + (2.512 \times 10^3)(168 - 127)(0.695)]}\right\}^{1/2}$$
$$= 2.6885 \times 10^{-3}\,\text{kg/m} \cdot \text{s}$$

which is equivalent to a total rate of melting of 0.00872 in^3/s, or only about 3% below the measured value.

The close agreement between the predictions and the measured rates of melting is to some degree fortuitous because all the thermophysical properties were selected from the literature rather than measured on the particular grade of HDPE used in the experiments. Thermophysical property data can vary for the same polymer over a relatively broad range. In addition, no doubt, experimental errors were also involved in the measured data, and one cannot expect perfect agreement. Nevertheless, it is reasonable to conclude that the *theoretical models* discussed in this section *predict correctly* the change in melting rate with changing experimental conditions, and that they provide *reasonable estimates* of the rate of melting.

Incorporating both the effect of convection in the film and the temperature dependence of the viscosity into the model improves the agreement between predictions and experimental measurements. It should be noted, however, that experimental conditions were such that viscous dissipation was insignificant and the temperature drop across the film was relatively small. Consequently, non-Newtonian effects, and effects due to the temperature dependence of viscosity, were less significant than were convection effects. This may not be the case in many practical situations, in particular with polymers, whose viscosity is more temperature sensitive than that of HDPE.

5.8 PRESSURE-INDUCED MELT REMOVAL

In the pressure-induced process, the melt is removed by the squeezing action of the solid on the melt; hence, the *force* by which the solids are pushed against the hot surface becomes the dominant rate-controlling variable. This melting process is less important in polymer processing than the drag removal process. Nevertheless, as Stammers and Beek (37) point out, in manufacturing certain synthetic fibers (e.g., polyester yarns) the polymer is melted on a melting grid; the melting process on such a melting grid is that of pressure removal of the melt. Stammers and Beek developed the following approximate theoretical model for the melting process.

Consider a polymer bar of radius R pressed by force F_N against a hot metal bar at constant temperature T_b of the same radius, as in Fig. 5.13. A film of melt is formed that is being squeezed out by radial flow.

The following simplifying assumptions are made:

1. The solid is rigid and moves with constant velocity toward the hot bar.
2. The film between the polymer and the hot bar has a constant thickness, δ.
3. Flow in the film is laminar.
4. The fluid is Newtonian.
5. Viscosity is temperature independent.
6. Thermophysical properties are constant.
7. Steady state.
8. Gravitational forces are negligible.
9. Convection and viscous dissipation on the film are negligible.

Some of these assumptions may be questionable, for example, the assumptions that the solid is rigid and the film thickness constant. In reality, as the preceding section

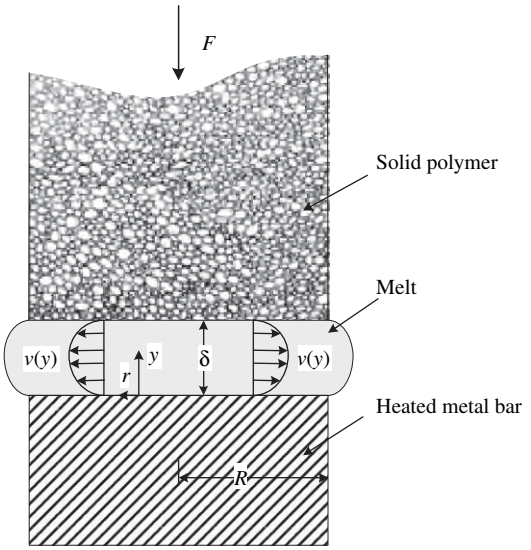

Fig. 5.13 Schematic representation of a solid polymer melting on a hot metal bar.

demonstrated, allowing the solid to deform and using an a priori unknown $\delta(r)$ would be more plausible. Nevertheless the foregoing assumptions do allow the ''construction'' of a simple model for the process, providing insight into its nature. Moreover, the model did show reasonably good agreement with experiments carried out with polyethylene and polyoxymethylene.

With the rigid polymer assumption, the total rate of melting can immediately be written as

$$w_T = \pi(-v_{sy})\rho_s R^2 \tag{5.8-1}$$

where $v_{sy} < 0$ is the velocity of the solid polymer. Our objective is to find a relationship between the velocity v_{sy}, the operating conditions (the pushing force F_N, the hot plate, and solid temperatures), and the polymer physical properties.

By pressing the bar against the plate, a radial velocity profile will be induced in the melt film, thus removing the newly melted polymer from the location of melting, and draining it. The mean radial velocity at any location r, v_r can be expressed in terms of (the yet unknown) velocity v_{sy} by a simple mass balance

$$\rho_s \pi r^2(-v_{sy}) = 2\pi r\delta\bar{v}_r\rho_m \tag{5.8-2}$$

where δ is the local separation between the interface and plate. Thus from Eq. 5.8-2 the mean radial velocity with $\beta = \rho_s/\rho_m$ is

$$\bar{v}_r = \frac{r(-v_{sy})\beta}{2\delta} = \frac{1}{\delta}\int_0^{\delta} v_r\, dy \tag{5.8-3}$$

The radial component of the equation of motion reduces to

$$\frac{dP}{dr} = \mu \frac{d^2 v_r}{dy^2} \tag{5.8-4}$$

We have substituted ordinary differentials for the partial differentials in the equation of motion because the left-hand side is only a function of r, whereas we assume the right-hand side is only a function of y (lubrication approximation). Therefore, they simply equal a constant. Equation 5.8-4 can now be integrated over y, with boundary conditions $v_r(0) = 0$ and $v_r(\delta) = 0$, to give

$$v_r = \frac{1}{2\mu} \frac{dP}{dr} (y - \delta) y \tag{5.8-5}$$

An expression for the pressure gradient dP/dr versus r can be obtained by substituting Eq. 5.8-5 into Eq. 5.8-3

$$-\left(\frac{dP}{dr}\right) = \frac{6\mu(-v_{sy})r\beta}{\delta^3} \tag{5.8-6}$$

Integration of Eq. 5.8-6 with the boundary condition $P(R) = P_0$, where P_0 can be the atmospheric pressure, leads to the following pressure profile:

$$P(r) - P_0 = \frac{3\mu(-v_{sy})\beta}{\delta^3} \left(R^2 - r^2\right) \tag{5.8-7}$$

The total force F_N can be calculated from the pressure profile:

$$F_N = \int_0^R 2\pi r P(r)\, dr = \pi R^2 P_0 + \left(\frac{3\mu\pi(-v_{sy})R^4\beta}{2\delta^3}\right) \tag{5.8-8}$$

Equation 5.8-8 is, in effect, the relationship we are looking for, and by rearranging it we get a relationship of the velocity v_{sy} in terms of the external total force F_N and a number of other variables

$$(-v_{sy}) = \frac{2\delta^3(F_N - \pi P_0 R^2)}{3\pi\mu R^4 \beta} \tag{5.8-9}$$

We cannot, however, calculate the melting rate of this geometrical configuration from Eq. 5.8-9 because we do not yet know the value of δ. This value is determined by the rate of heat conducted into the solid–melt interface. If we make use of one more of the simplifying assumptions just given, namely, that viscous dissipation is negligible, the following simple heat balance can be made on the interface (see Eq. 5.7-14)

$$k_m\left(\frac{T_b - T_m}{\delta}\right) = \rho_s(-v_{sy})[\lambda + C_s(T_m - T_b)] \tag{5.8-10}$$

where T_0 is the initial temperature of the solid. Substituting Eq. 5.8-9 into Eq. 5.8-10 results in the final expression, which is the process-design equation

$$(-v_{sy}) = \frac{0.6787}{R}\left(\frac{F_N - \pi P_0 R^2}{\mu\beta}\right)^{1/4}\left[\frac{k_m(T_b - T_m)}{\rho_s[\lambda + C_s(T_m - T_0)]}\right]^{3/4} \tag{5.8-11}$$

The melting capacity of this geometrical configuration can easily be calculated from Eqs. 5.8-11 and 5.8-1.

The results are very revealing and instructive. The rate of melting increases with the total force F_N, but only to the one fourth power. The physical explanation for this is that with increasing force, the film thickness is reduced, thus increasing the rate of melting. However, the thinner the film, the larger the pressure drops that are needed to squeeze out the melt. The dependence on the plate temperature is almost linear. The inverse proportionality with R is perhaps the most important result from a design point of view. If viscous dissipation were included, some of these results would have to be modified.

Stammers and Beek (37) have performed a number of experiments to verify the theoretical model just described, using polyethylene and polyoxymethylene. The linear relationship between $v_{sy}/(F_N)^{1/4}$ and $[(T_b - T_m)^{3/4}/\mu^{1/4}]$, as predicted by Eq. 5.8-11, was clearly established, and the slope calculated from this equation agreed well with the experimental data.

5.9 DEFORMATION MELTING

It is evident from the foregoing discussion that considerable effort has been invested in elucidating the mechanism of conduction melting, and in particular that of conduction melting with forced drag flow melt removal, the latter because it is the operative melting mechanism in single-rotor processing equipment such as SSEs and injection-molding machines. We will discuss in detail the utilization of this melting mechanism in the modeling of single-rotor melting in Chapter 9, a task that proves to be rather straightforward, due to the ordered segregation of the two polymer phases involved: the flowing molten polymer, and the ‘‘passive,’’gradually melting, compacted particulate ‘‘bed.’’

On the other hand, we discussed and presented in physical terms the very powerful melting mechanisms resulting from repeated, large deformations, forced on compacted particulate assemblies by twin co- or counterrotating devices. These mechanisms, which we refer to in Section 5.1, are *frictional energy dissipation* (FED), *plastic energy dissipation* (PED), and *dissipative mix-melting* (DMM).

At the time of the writing of the first edition of this text (38), we wrote the following about mechanical energy dissipation in repeatedly deforming "active" compacted particulates and the evolution of their melting:

> . . . the dominant source of energy for melting (in twin rotor devices) is mechanical energy introduced through the shafts of the rotors and converted into thermal energy by continuous gross deformation of the particulate charge of polymer . . . by a number of mechanisms: individual particle deformations [now known as PED (3)], inter-particle friction [now known as

> FED (3)] and viscous dissipation in the molten regions. As melting progresses the latter mechanism becomes dominant. Mixing disperses the newly formed melt into the mass [creating a solids-rich suspension]; the melt that comes in intimate contact with solid particles cools down and at the same time heats up the surface layer of the particles; the particulate solid charge is eventually converted into a richer, thermally inhomogeneous suspension and ultimately into a homogeneous one. . . . Nevertheless, the advantages of this melting method dictate that more theoretical [and experimental] analysis be devoted to it in the near future.

Indeed, over the last decade, the area of melting of active compacted particulate assemblies in twin-rotor equipment has received a good deal of experimental attention. This body of experimental work utilizes both glass windows on sections of the barrel for on-line observations (39–43) and, more often, extracted solidified ''carcasses'' of the processed stream, which are sectioned along the downstream direction in the melting region (3,44–50). This body of work has confirmed the existence, and elucidated the natures of PED, FED, and DMM and, most importantly, has confirmed the evolution of melting in twin-rotor devices mentioned earlier. Such evolution, based on extensive ''carcass'' analyses for both polypropylene (PP) pellets and powder feeds in Co-TSEs, is shown in Fig. 5.14 (3,51).

As seen in the figure, the successive downstream states of the PP pellets as they are conveyed, consolidated, and melted, result from PED, VED, and DMM taking place throughout the volume of the processed stream. The small size of the 30-mm-diameter

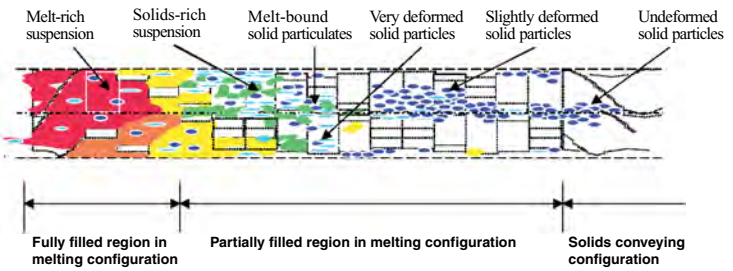

States of the stream				
Schematic representation				
Co-TSE screw configuration				
VED	PED VED (DMM)	PED (FED)	Conduction	Melting mechanisms (pellets)
VED	PED VED (DMM)	PED FED	Conduction	Melting mechanisms (powder)

Fig. 5.14 Schematic representation of the evolution of melting of polypropylene (PP) pellets in a 30-mm-diameter co-TSE. The figure represents rendition of the analyses of many experimental carcasses. Shown are: the physical states of the pellets stream being melted; a schematic of the carcass ''morphology''; the screw conveying/kneading element sequence; and the melting mechanisms responsible for affecting melting of the pellets stream. Shown in the bottom row are the melting mechanisms responsible for advancing melting of a polypropylene powder feed. [Reprinted by permission from M. H. Kim, Ph.D Dissertation Department of Chemical Engineering, Stevens Institute of Technology, Hoboken. NJ., (1999).]

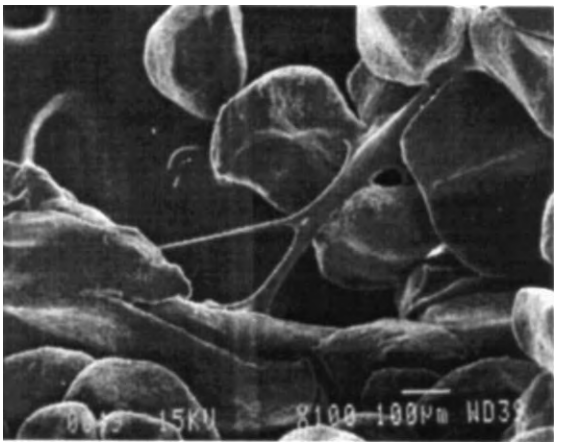

Fig. 5.15 Evidence of melting of fine particulates of PP powder melted in a 30-mm Co-TSE, taking place in the partially filled kneading section. Such molten fines are capable of creating, as glue points, particulate clusters. [Reprinted by permission from M. Esseghir, D. W. Yu, C. G. Gogos, and D. B. Todd, *SPE ANTEC Tech Papers*, **43**, 3684 (1997).]

split-barrel extruder with a maximum channel depth of 4 mm causes pellets to be deformed, that is, undergo PED, even in partially filled sections upstream of the consolidated particulates melting zone.

Carcasses of PP powder feed (not shown in Fig. 5.14) do show clear evidence of the melting of single particulates by FED, becoming local ''glue points'' and creating clusters of powder particulates, as shown in Fig. 5.15. Further evidence of FED was provided by Shih et al. (39) working with a glass end-plate Brabender Plasticorder melting powder charges. Gogos et al. (51) investigated the melting behavior of three PP powder systems using Shih's experimental device. The three powder systems differed in concentration of fine particulates. The fines-rich system exhibited very early and fast evidence of cluster formation: the power generated by neighboring particulates moving at different speeds (Δv) while under a normal force F_N is

$$p_w = fF_N \Delta v \tag{5.9-1}$$

where f is the interparticle coefficient of friction. Small particulates wedged between larger ones in the ''nip'' compressing region between the rotors will melt first by FED, because of their large surface-to-volume ratio.

We now turn our attention to PED. As mentioned earlier, individual pellets become grossly deformed while in compacted assemblies, for example, in kneading sections of the Co-TSE. These volumewise particulate deformations make the particulate assemblies active participants in the process of melting through the mechanism of PED. Two questions must be addressed: (a) how powerful a heat source term is PED? and (b) how can the complex reality of compacted particulate assemblies undergoing large and repeated deformations be described and simulated mathematically?

We know from our discussion of deforming particulate ''beds'' in Chapter 4 that the answer to the second question, that is, the quantification of PED in deforming assemblies,

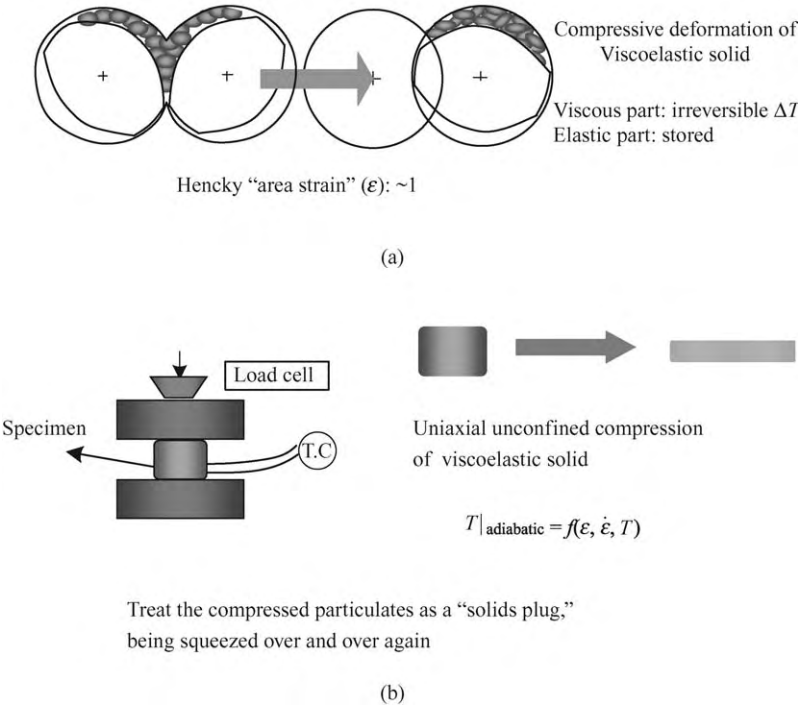

Fig. 5.16 Schematic representation of (a) a compacted pellet assembly undergoing kneading (squeezing) deformations as the pair of kneading paddles co-rotates, reducing the available volume, forcing them to move into connecting spaces of neighboring down- and upstream kneading element pairs; (b) a single molded disk undergoing unconfined compressive deformation, used by Gogos et. al. (3) to represent the ''complex'' physical reality shown in (a) and estimate the resulting actual PED. [Reprinted by permission from M. H. Kim, Ph.D Dissertation, Department of Chemical Engineering, Stevens Institute of Technology, Hoboken, NJ, (1999).]

is not available to date because of the complexity of the physical phenomena involved. For this reason, Kim (52) and Gogos et al. (3) decided to probe and elucidate the physical nature and magnitude of PED by measuring or estimating the adiabatic temperature rise in single molded-polymer disks undergoing rapid, unconfined compressive deformations. The complexity of deforming particulate assemblies by kneading Co-TSE elements are shown side by side with the simplicity of the experiments conducted by Kim and Gogos in Fig. 5.16 (52).

Typical results obtained during unconfined compressive deformation experiments using direct thermocouple measurements—a difficult experimental task—are shown in Fig. 5.17. A number of the results are important: the magnitude of the increases in the observed specimen temperature is significant; temperature increases are negligible in the initial elastic deformation region, as expected; and the magnitude of the measured ''adiabatic''temperature rise ΔT_a increases with the strength of the polymer because of the higher deformation stresses. Thus, for strong amorphous polymers below T_g, such as PS, the observed ΔT_a values are almost one order of magnitude larger than those obtained with semicrystalline polymers at temperatures between T_g and T_m. It was found experimentally that the measured ΔT_a values can be closely approximated by relating the

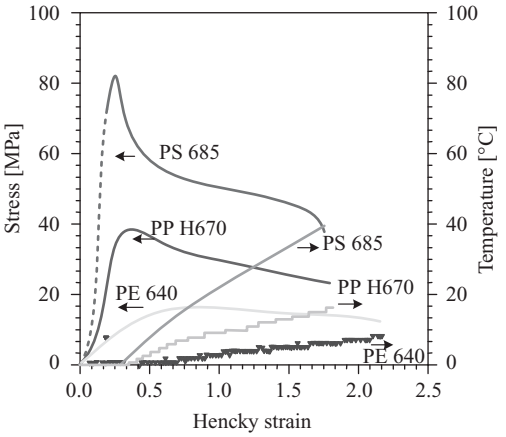

Fig. 5.17 Unconfined compression stress–strain curves and experimentally measured temperature increase ΔT_a as a function of strain for PS (Dow 685), LDPE (Dow 640), and PP (LG H670). The initial test specimen was at 26°C and the crosshead speed of the compressing bar with the load cell was 25.4 mm/min. The specimen dimensions were: 101 mm diameter and 71 mm height. [Reprinted by permission from M. H. Kim, Ph.D Thesis, Department of Chemical Engineering, Stevens Institute of Technology, Hoboken, NJ (1999).]

''area'' under the stress–strain curve with the adiabatic specific enthalpy increase during compression

$$\text{PED} = \int_{\varepsilon_e}^{\varepsilon} \sigma d\varepsilon = \rho C_p \Delta T_a \tag{5.9-2}$$

or

$$\Delta T_a = \frac{\int_{\varepsilon_e}^{\varepsilon} \sigma \, d\varepsilon}{\rho C_p} \tag{5.9-3}$$

Note that, since the stress–strain curves are dependent on the applied strain rate and the specimen temperature, both PED and ΔT_a are functions of the strain, strain rate, and temperature.

Kim (52) conducted a large number of compressive deformation experiments using specimens at increasingly higher initial temperatures at the highest experimental strain rate available to the universal testing machine used. With these data he constructed iso-PED curves in the Hencky strain–initial specimen temperature space, shown in Fig. 5.18(a). Excellent estimates of the PED generated on PS disks of any initial temperature above room temperature undergoing deformation to any strain $\varepsilon < 1.6$ at 25.4 cm/s can thus be obtained. Furthermore, using Eq. 5.9-2 the iso-PED results can be transformed to the so ΔT_a curves shown in Fig. 5.18(b). Using this figure, one can get a good estimate of how much the initial temperature of a PS will increase after successive $\varepsilon_{\text{Hencky}} = 1$ deformations, as indicated in Fig. 5.19.

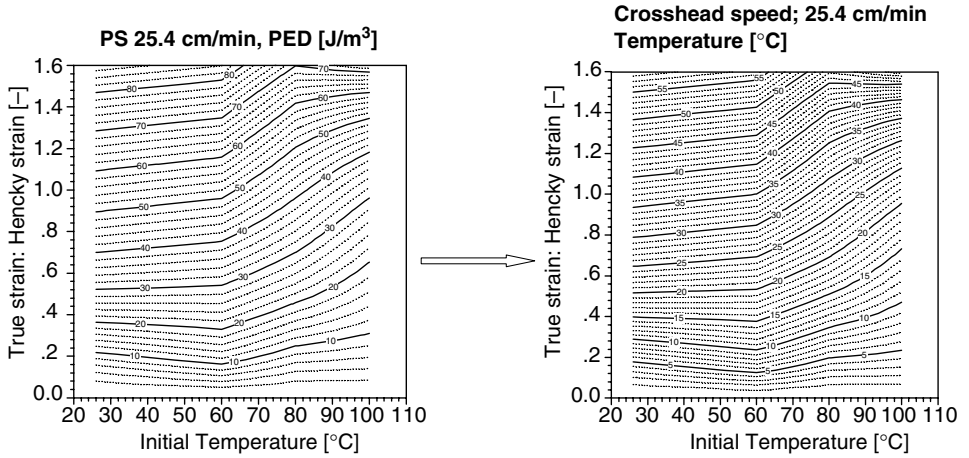

Fig. 5.18 (a) Iso-PED (J/m^2) curves obtained from unconfined compressive deformation experiments of Dow PS 685 cylindrical specimens compressed at 25.4 cm/min. Many experiments were conducted for a number of initial specimen temperatures (T_i) and with a number of applied strains at each T_i. (b) iso ΔT_a (°C) for PS 685 derived from curves in part (a) employing the relation $\Delta T|_{\varepsilon_0,T_i} = \text{PED}/\rho\bar{C}_p$. [Reprinted by permission from M. H. Kim, Ph.D. Thesis, Department of Chemical Engineering, Stevens Institute of Technology, Hoboken, NJ (1999).]

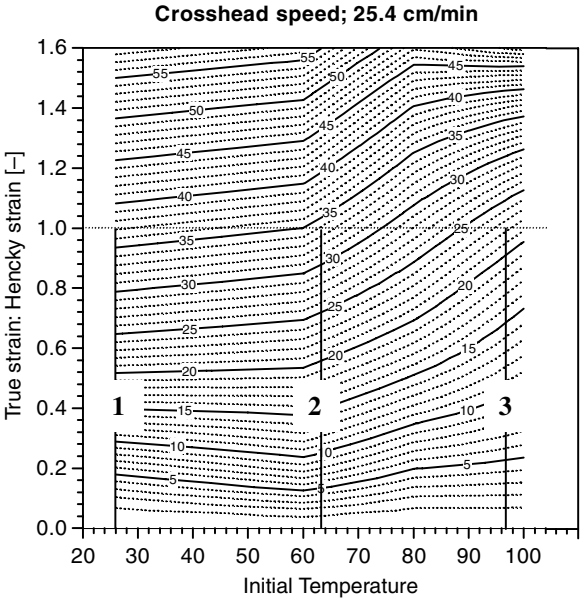

Fig. 5.19 The effect of consecutive unconfined compressive deformations on the temperature increase of a PS cylinder initially at 26°C. The first $\varepsilon = 1$ deformation increases for sample temperature by 37°C; the second starting from $26 + 37 = 63\,^{\circ}\text{C}$, increases it to 97°C, close to T_g. [Reprinted by permission from M.H. Kim, Ph.D. Thesis, Department of Chemical Engineering, Stevens Institute of Technology, Hoboken, NJ (1999).]

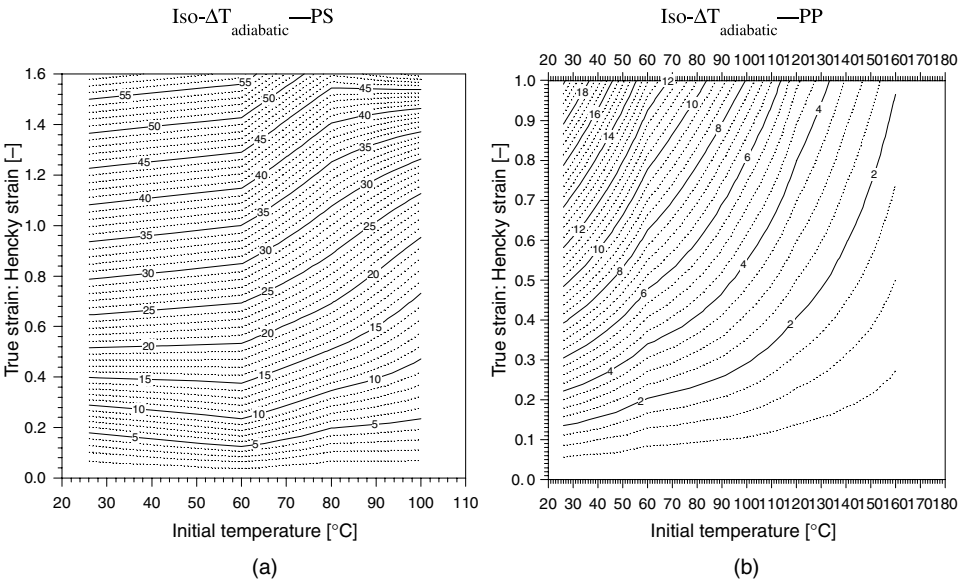

Fig. 5.20 The PED for PP is apparently smaller in magnitude than that for PS; it is also more temperature dependent, decreasing with increasing initial temperature. Semicrystalline plastics are weaker and their amorphous phase in the region $T > T_g$ becomes more mobile, rapidly lowering the needed deformation stresses. [Reprinted by permission from M.H. Kim, Ph.D. Thesis, Department of Chemical Engineering, Stevens Institute of Technology, Hoboken, NJ (1999).]

After the first $\varepsilon = 1$ deformation, the initial sample temperature (26°C) will increase by 37°C to $(26^\circ + 37^\circ) = 63^\circ$C. After the second deformation, the new sample temperature will be $63^\circ + 34^\circ = 97^\circ$C. It is striking that only two successive compressive $\varepsilon = 1$ deformations are capable of raising the PS sample temperature very close to T_g. The conclusion from such experimental findings, which we will discuss further in connection with twin rotor devices in Chapter 10, is that PED is a very powerful melting mechanism for PS.

Similar experiments were conducted to evaluate the magnitude of PED in semicrystalline polymers in the region $T_{\text{room}} < T < T_m$. Iso-PED and iso-$\Delta T_a$ curves for Dow LDPE 640 are shown in Fig. 5.20(a) and 5.20(b). These curves show dramatic differences when compared to those for PS: not only the *magnitude* of the PED and, consequently, the ΔT_a values are *smaller*, for example, for PS at an initial temperature of 26°C after $\varepsilon = 1, \Delta T_a = 37^\circ$C, while for LDPE it is only 10°C, but the *temperature sensitivity* of PED is much stronger for LDPE, so much so that at an initial temperature of 80°C for PS, it is 27°C, while for LDPE, it is only 4°C.

The physical origin for this difference is indicated in Fig. 5.21: amorphous polymers below T_g exhibit a constant modulus, since they are single-phase, rigid-chain structures, while semicrystalline, two-phase structures in the range $T_g < T < T_m$ become weaker with increasing temperature, due to the increased mobility of the amorphous chains.

The theoretical models that have been proposed to quantify and simulate the melting phenomena taking place in ‘‘active’’ compacted particulates are still rudimentary, not for lack of effort and interest, but because of the physical complexities involved, as noted

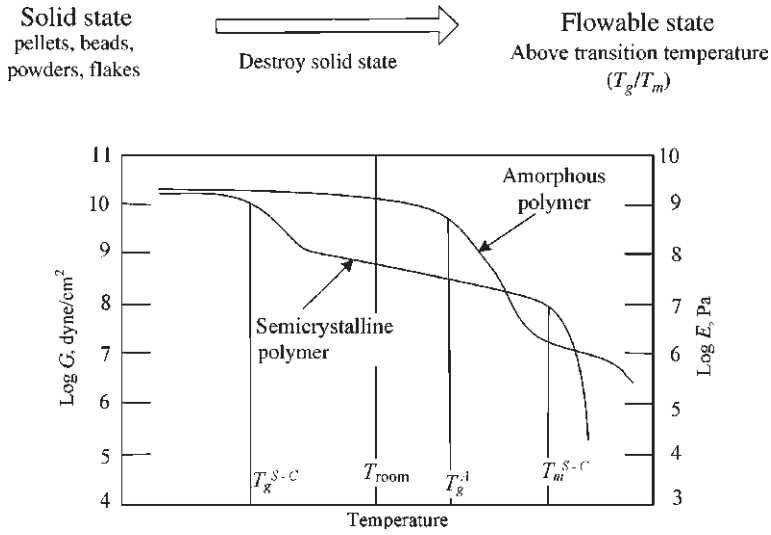

Fig. 5.21 Polymer feed temperatures are at or near T_{room}. For common amorphous plastics, $T_{\text{room}} < T_g$, and for semicrystalline $T_g < T_{\text{room}} < T_m$. As disussed in the text, PED, through large solid-state irreversible deformations, makes the solid an ''active participant'' in the melting process, rapidly creating a molten state. The modulus of amorphous polymer is higher and less temperature dependent in the region $T > T_{\text{room}}$. Consequently, the magnitude of amorphous PED is larger and less temperature dependent when compared to semicrystalline PED.

earlier. Vergnes et al. (53) concur with the foregoing analysis and suggest that ''Gogos et al. (3) showed the important roles of pellets plastic deformation and interparticle friction, which modify (i.e., should be included in) the thermal energy balance.'' These phenomena, they continue, ''should probably be taken into account in heat generation for melting. However, it remains difficult to quantify properly these terms, and the lack of physical data makes it difficult to introduce them in a model.''

Potente and Melish (49), Vergnes et al. (53), Bawiskar and White (54), and Zhu et al. (55) have proposed simulation models to describe melting in the Co-TSEs. These models are all based on the assumption that melting occurs mainly by VED during the flow of suspensions of solid polymer particulates in melts, with the evolution of melting involving the decrease in the size of the particulates. In Chapter 10 we will review the model of Vergnes et al., the PED-based model of Gogos et al. (56) and Kim and Gogos (57), and one by Jung and White (58), The latter two consider the PED contributions to melting in full Co-TSE kneading elements.

REFERENCES

1. T. K. Ross, ''Heat Transfer to Fusible Solids,'' *Chem. Eng. Sci*., **1**, 212–215 (1952).
2. G. Menges and W. Elbe, ''Untersuchungen des Einzugsand Plastifizierverhaltens von Schneckenspritzgiessmachinen,'' Beitrag zum 5, Kunstofftechnischen Kolloquium des Institut fur Kunstoffverarbeitung, Aachen, Germany, 1970.
3. C. G. Gogos, Z. Tadmor, and M. H. Kim, ''Melting Phenomena and Mechanisms in Polymer Processing Equipment,'' *Adv. Polym. Technol*., **17**, 285–305 (1998).

4. L. Erwin and N. P. Suh, ‘‘A Method for the Rapid Processing of Thermoplastic Articles,’’ *Polym. Eng. Sci*., **16**, 841–846 (1976).
5. E. R. G. Eckert and R. M. Drake, Jr., *Analysis of Heat Transfer*, McGraw-Hill, New York, 1972: (a) p. 219; (b) p. 157; (c) p. 12.
6. T. R. Goodman, ‘‘Application of Integral Methods for Transient Nonlinear Heat Transfer,’’ in *Advances in Heat Transfer*, Vol. I, T. F. Irvine, Jr., and J. P. Hartnett, Eds., Academic Press, New York, 1964, pp. 51–122.
7. S. G. Bankoff, ‘‘Heat Conduction or Diffusion with Change in Phase,’’ in *Advances in Chemical Engineering*, Academic Press, New York, 1964, pp. 75–100.
8. L. I. Rubinstein, ‘‘The Stefan Problem,’’ in *Translation of Mathematical Monographs*, Vol. 27, American Mathematical Society, Providence, RI, p. 5, 1971.
9. S. W. Churchill and L. B. Evans, ‘‘Coefficients for Calculation of Freezing in a Semi-infinite Region,’’ *Trans. Am. Soc. Mech. Eng., J. Heat Transfer*, **93**, 234–236 (1971).
10. H. S. Carslaw and J. C. Jaeger, *Conduction of Heat in Solids*, Second Edition, Oxford University Press, New York, 1959.
11. W. M. Rosenhow and J. P. Hartnett, *Handbook of Heat Transfer*, McGraw-Hill, New York, 1973.
12. J. Eisenberg and G. deVahl Davis, ‘‘FDM Methods in Heat Transfer,’’ in *Topics in Transport Phenomena*, C. Gutfinger, Ed., Wiley, New York, 1975.
13. G. E. Myers, *Analytical Methods in Conduction Heat Transfer*, McGraw-Hill, New York, 1971, Chapter 8.
14. A. M. Clausing, ‘‘Numerical Methods in Heat Transfer,’’ in *Advanced Heat Transfer*, B. T. Chao, Ed., University of Illinois Press, Urbana, 1969, pp. 157–216.
15. G. M. Dusinberre, *Heat Transfer Calculations by Finite Differences*, Second Edition, International Textbook, Scranton, PA., 1961.
16. J. Crank and P. Nicolson, ‘‘A Practical Method for Numerical Evaluation of Solutions of Partial Differential Equations of the Heat-conducting Type,’’ *Proc. Cambridge. Philos. Soc*., **43**, 50–67 (1947).
17. D. Rosenthal, ‘‘A Theory of Moving Sources of Heat and its Application to Metal Treatment,’’ *Trans. Am. Soc. Mech. Eng*., **68**, 849–866 (1946).
18. G. C. Kuczynski, B. Neuville, and H. P. Toner, ‘‘Study of Sintering of Poly(Methyl Methacrylate)’’, *J. Appl. Polym. Sci*., **14**, 2069–2077 (1970).
19. M. A. Rao and J. L. Throne, ‘‘Principles of Rotational Molding,’’ *Polym. Eng. Sci*., **12**, 237–250 (1972).
20. J. L. Throne, ‘‘Rotational Molding Heat Transfer – an Update,’’ *Polym. Eng. Sci*., **16**, 257–264 (1976).
21. J. F. Lonz, ‘‘Sintering of Polymer Materials,’’ in *Fundamental Phenomena in the Material Sciences*, Vol. 1, *Sintering and Plastic Deformation*, L. J. Bonis and H. H. Hausner, Eds., Plenum Press, New York, 1964.
22. D. M. Bigg, ‘‘High Pressure Molding of Polymeric Powders,’’ Proc. of the Society of Plastics Engineers 33rd Annu. Tech. Conf., Atlanta, May 1975, pp. 472–476.
23. G. S. Jayaraman, J. F. Wallace, P. H. Geil, and E. Baer, ‘‘Cold Compaction Molding and Sintering of Polystyrene,’’ *Polym. Eng. Sci*., **16**, 529–536 (1976).
24. J. Frenkel, *J. Phys. (U.S.S.R)*, **9**, 385 (1945).
25. J. D. Eshelby, *Trans. Am. Inst. Mech. Eng*., **185**, 806 (1949).
26. D. H. Sundstrom and J. R. Lo, ‘‘Softening Rates for Polystyrene under Shear Conditions,’’ *Polym. Eng. Sci*., **18**, 422 (1978).

27. Z. Tadmor, ‘‘Fundamentals of Plasticating Extrusion. I. A Theoretical Model for Melting,’’ *Polym. Eng. Sci*., **6**, 185–190 (1966). First presented at the Society of Plastics Engineers Annual Technical Conference, Montreal Canada, April 1966.
28. Z. Tadmor, I. J. Duvdevani, and I. Klein, ‘‘Melting in Plasticating Extruders Theory and Experiments,’’ *Polym. Eng. Sci*., **7**, 198–217 (1967).
29. Z. Tadmor and I. Klein, *Engineering Principles of Plasticating Screw Extrusion*, Van Nostrand Reinhold, New York, 1970.
30. Z. Tadmor and I. Klein, ‘‘Melting in Plasticating Extruders’’ in I. Klein and D. I. Marshall, Eds., *Computer Programs for Plastics Engineers*, Reinhold, New York, 1968, Chapter 6.
31. Z. Tadmor, ‘‘Machine Invention, Innovation, and Elementary Steps,’’ *Adv. Polym. Technol*., **21**, 87–97 (2002).
32. J. R. Vermeulen, P. M. Gerson, and W. J. Beek, ‘‘The Melting of a Bed of Polymer Granules on a Hot Moving Surface,’’ *Chem. Eng. Sci*., **26**, 1455 (1971).
33. D. H. Sundstrom and Chi-Chang Young, ‘‘Melting Rates of Crystalline Polymers under Shear Conditions,’’ *Polym. Eng. Sci*., **12**, 59–63 (1972).
34. E. M. Mount, III, ‘‘The Melting of High Density Polyethylene on a Heated, Moving Metal Surface—A Comparison of Experimental and Theoretical Results,’’ M.S. thesis, Rensselaer Polytechnic Institute, Troy, NY, (1976).
35. J. R. A. Pearson, ‘‘On the Melting of Solids near a Hot Moving Interface, With Particular Reference to Beds of Granular Polymers,’’ *Int. J. Heat Mass Transfer*, **19**, 405–411 (1976).
36. T. R. Fuller and A. L. Fricke, ‘‘Thermal Conductivity of Polymer Melts,’’ *J. Appl. Polym. Sci*., **15**, 1729–1736 (1971).
37. E. Stammers and W. J. Beek, ‘‘The Melting of a Polymer on a Hot Surface,’’ *Polym. Eng. Sci*., **9**, 49–55 (1969).
38. Z. Tadmor and C. G. Gogos, *Principle of Polymer Processing*, Wiley, New York, 1979, Chapter 9.
39. C. K. Shih, D. G. Tynan, and D. A. Denelsbek, ‘‘Rheological Properties of Multicomponent Polymer Systems Undergoing Melting or Softening during Compounding,’’ *Polym. Eng. Sci*., **31**, 1670 (1991).
40. N. Hashimoto, J. Kakizaki, *JPS Tech. Rev*., **16**, 48 (1994).
41. T. Sakai, ‘‘The Development of On-line Techniques and Novel Processing Systems for the Monitoring and Handling of the Evolution of Microstructure in Nonreactive and Reactive Polymer Systems,’’ *Adv. Polym. Techn*., **14**, 277 (1995).
42. A. C. Y. Wong, F. Zhu, and T. Liu, ‘‘Qualitative Study on Intermeshing Co-rotating Twin Screw Extrusion Using Novel Visual Technique,’’ *Plast. Rubber Comps. Proc. Appl*., **26**, 271 (1997).
43. L. Zhu and X. Geng, ‘‘Visual Research of Melting Mechanism of Polymer Pellets in Intermeshing Co-rotating Twin-screw Extrusion,’’ *SPE ANTEC Tech. Papers*, **55**, 3684 (1997).
44. D. B. Todd, ‘‘Melting of Plastics in Kneading Blocks,’’ *Int. Polym. Proc*. **8**, 113 (1993).
45. J. Curry, ‘‘Melting Mechanisms in ZSK Extruders,’’ *SPE ANTEC Tech. Papers*, **41**, 92 (1995).
46. H. T. Chan and D. A. DuFresne, ‘‘Kneading Block Melting Study,’’ *SPE ANTEC Tech. Papers*, **53**, 302 (1995).
47. F. Busby, T. W. McCullough, K. R. Hugues, and R. O. Kirk, ‘‘Melting of Homopolymers in Co-rotating, Intermeshing Twin-screw Extruders,’’ *SPE ANTEC Tech. Papers*, **54**, 3571 (1996).
48. M. Esseghir, D. W. Yu, C. G. Gogos, and D. B. Todd, ‘‘Melting Mechanisms of Single-component Polymers in Co-rotating Twin-Screw Kneading Blocks Through Visual and Microscopic Analysis,’’ *SPE ANTEC Tech. Papers*, **43**, 3684 (1997).

49. H. Potente and U. Melish, "Theoretical and Experimental Investigations of the Melting of Pellets in Co-rotating Twin-screw Extruders," *Int. Polym. Proc*., **11**, 101 (1996).
50. S. Bawiskar and J. L. White, "A Composite Model for Solid Conveying, Melting, Pressure and Fill Factor Profiles in Modular Co-rotating Twin Screw Extruders," *Int. Polym. Proc*., **12**, 1331 (1997).
51. C. G. Gogos, M. Esseghir, D. W. Yu, D. B. Todd and J. Curry, "The Twin-screw Mixing Element Evaluator: On-line Performance Evaluation of Modular Twin-screw Mixing Elements," *SPE ANTEC Tech. Papers*, **40**, 270 (1994).
52. M. H. Kim, Ph.D. Dissertation, Deptartment of Chemical Engineering, Stevens Institute of Technology, Hoboken, NJ, (1999).
53. B. Vergnes, G. Souveton, M. L. Delacour, and A. Ainser, "Experimental and Theoretical Study of Polymer Melting in a Co-rotating Twin Screw Extruder," *Int. Polym. Process*., **16**, 351–362 (2001).
54. S. Bawiskar and J. L. White, "Melting Model for Modular Self Wiping Co-rotating Twin Screw Extruders," *Polym. Eng. Sci*., **38**, 727 (1998).
55. L. Zhu, K. A. Narh, and X. Geng, "Modeling of Particle-dispersed Melting Mechanism and its Application in Corotating Twin-screw Extrusion," Paper presented at the 17th Polymer Processing Society Meeting, Montreal, Canada (2001).
56. G. Gogos, B. Qian, D. B. Todd, and M. H. Kim, "A Predictive Melting Model for Polymer Particulates in Co-TSE's," *SPE ANTEC Tech. Papers*, **47**, 134 (2001).
57. M. H. Kim and C. G. Gogos, "Melting Phenomena and Mechanisms in Co-TSEs," *SPE ANTEC Tech. Papers*, **47**, 145 (2001).
58. H. Jung and J. L. White, "Investigations of melting Phenomena in Modular Co-rotating Twin Screw Extrusion," *Int. Polym. Process*., **18**, 127 (2003).

PROBLEMS

5.1 ***Feeding a Metal Strip into a Hot Oven*** A thin metal strip of thickness δ and width W is fed at a constant speed V_0 into a hot furnace at temperature T_f, as shown in the figure. Find the minimum distance L where the feeding roll can be placed, such that the strip temperature should not exceed T_1, while the room temperature is T_0 and $T_1 > T_0$. Assume that the strip temperature at $x = 0$ equals the furnace temperature, and that heat transfer is uniaxial in the x direction (no heat losses).

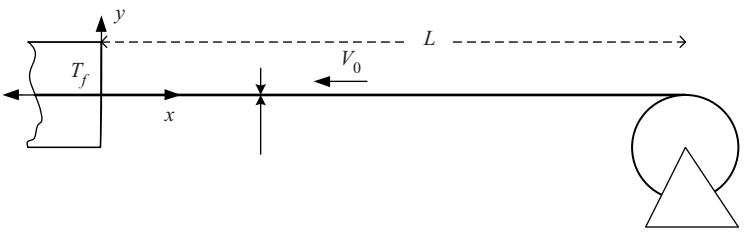

5.2 ***Here Are the Answers. What Were the Questions?*** (a) Different operators got different readings because they immersed the thermometer for different periods of time. (b) After immersing the bulb for time $t = MC_p/hA$, the dimensionless

temperature $\theta = (T_f - T)/(T_f - T_i)$ reached $1/e$, and after twice that time $1/e^2$, where T_f is the fluid temperature, T_i the initial temperature, M is the mass of the bulb, and h is the heat-transfer coefficient.

5.3 ***Solution of Heat Transfer Problems by Combination of Variables*** Show that the partial differential equation

$$\frac{\partial T}{\partial t} = \alpha \frac{\partial^2 T}{\partial x^2}$$

is reduced to the ordinary differential equation E5.2-3 by defining a new variable $\eta = Cxt^m$, where C and m are constants. Note that we combine the variables in such a way that $T = f(\eta)$, where $\eta = F(x, t)$. Use the Chain Rule to obtain expressions for $\partial T/\partial t$, $\partial T/\partial x$, and $\partial^2 T/\partial x^2$, then substitute for $\partial \eta/\partial t$, $\partial \eta/\partial x$, and $\partial^2 \eta/\partial x^2$.

5.4 ***Time-dependent Temperature Boundary Conditions*** (a) Consider the heat-transfer problem involved inside a semi-infinite solid of constant properties with a varying surface temperature:

$$T(0, t) = T_0 + A \cos(\omega t)$$

(b) Show that, with time, the relative amplitude of temperature $A_r = A(x)/A(0)$ is given by $A_r = \exp(-x\sqrt{\pi}/x_0)$ where $x_0 = \sqrt{2\pi\alpha/\omega}$. If the heat-transfer period equals the fluctuation period $2\pi/\omega$, then x_0 is a good estimate of the penetration thickness.
(c) Find the penetration thickness for a period of 100 s for LDPE, which has thermal diffusivity of $\alpha = 7 \times 10^{-}8\ \text{m}^2/\text{s}$.

5.5 ***Rotational Molding*** Throne et al.[4] investigated heat-transfer problems in rotational molding of polymeric powders. One of the simulation models for heat transfer they have considered is depicted in the accompanying figure. The lower

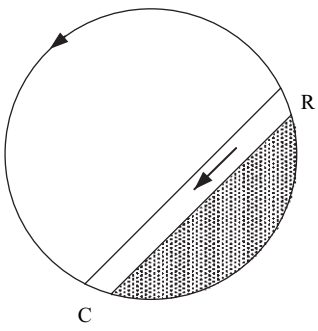

4. See M. Anandha Rao and J. L. Throne, "Principles of Rotational Molding," *Polym. Eng. Sci.*, **12**, 237 (1972).

(shaded) area represents a stagnant pool of polymer powder that undergoes rigid-body rotation with the rotating mold. When it reaches point R, it releases and falls back to C, where it is again heated by the hot mold wall. For each cycle, the time of contact is the time it takes for the mold to rotate from C to R. During the flowing stage, the powder is considered to be mixed thermally.

By following their work, using the Goodman method (6) and a temperature profile

$$T(x,t) = T_s\left(1 - \frac{x}{\delta(t)}\right)^3$$

where $T_s = T(0,t) = T_\infty\left(1 - e^{-\beta t}\right) + T^*$, with T_∞ the oven setpoint temperature, β the experimentally determined characteristic time of heating of the mold, and T^* the initial offset temperature, show that the penetration thickness $\delta(t)$ is given by

$$\delta(t) = \frac{2\sqrt{6\alpha_s}}{T_\infty(1 - e^{-\beta t_2}) + T^*}\left\{ t_c\left[T_\infty^2 + 2T_\infty T^* + T^{*2}\right]. \right.$$
$$+\left[\frac{2T_\infty^2}{\beta} + \frac{2T_\infty T^*}{\beta}\right]\left(e^{-\beta t_2} - e^{-\beta t_1}\right)$$
$$\left. -\frac{T_\infty^2}{2\beta}\left(e^{-2\beta t_2} - e^{-2\beta t_1}\right)\right\}^{1/2}$$

where $t_c = t_2 - t_1$ is the time of contact, $\alpha_s = \alpha$ at $x = 0$.

5.6 ***Dielectric Heating*** In dielectric heating, the rate of heat generated per unit volume for a field strength $\mathscr{F}$ of frequency f is

$$G = 13.3 \times 10^{-14} f \mathscr{F}^2 k' \tan\delta$$

where G is in cal/cm^{3}s, k' is the dielectric constant, and δ is the loss tangent. Derive the one-dimensional temperature profile $T(x)$ in a slab of width b and constant thermophysical properties with dielectric heating of intensity G. The slab is initially at a uniform temperature T_0 and $T(b) = T(-b) = T_0$.
Answer:

$$T - T_0 = \frac{G}{2k}\left\{(b^2 - x^2) - \frac{32b^2}{\pi^3}\sum_{n=0}^{\infty}\frac{1}{(2n+1)^2}\exp\frac{-\alpha(2n+1)^2\pi^2 t^2}{4b^2}\right.$$
$$\left.\times \sin\left[\frac{(2n+1)\pi}{2}\left(1 + \frac{x}{b}\right)\right]\right\}$$

5.7 ***Frictional Welding*** Two pieces of PMMA are to be welded frictionally. Estimate the normal pressure that has to be applied in order to raise the interface temperature from 25°C to 120°C in 1 s. The relative velocity between the sheets is 10 cm/s. The thermal conductivity of PMMA is 4.8×10^{-4} cal/cm · s, the thermal diffusivity is 9×10^{-4} cm^2/s, and the coefficient of friction is 0.5.

5.8 ***Fluidized-bed Coating of an Article*** A rectangular metal article with dimensions of $0.5 \times 5.0 \times 10.0$ cm is to be coated with PVC powder to a uniform coat thickness of 0.01 cm, using the fluidized-bed coating process. The fluidized-bed temperature is 20°C and the initial metal temperature is 150°C. (a) Assuming no convective losses to the fluidized bed, what would the metal temperature decrease need to be to form the desired coat thickness? (b) Estimate the effect of convective heat losses on the temperature decrease of the metal.

5.9 ***Parallel-Plate, Nonisothermal Newtonian Drag Flow with Constant Viscosity*** (a) Show that the temperature profile in steady drag flow of an incompressible Newtonian fluid between parallel plates at distance H apart, in relative motion V_0 and different constant temperatures, T_1 and T_2, assuming constant thermophysical properties and temperature independent viscosity, is given by

$$\frac{T - T_1}{T_2 - T_1} = \xi + \mathrm{Br}\xi(1-)\xi$$

where $\xi = y/H$ and Br is the Brinkman number defined as

$$\mathrm{Br} = \frac{\mu V_0^2}{k(T_2 - T_1)}$$

(b) Calculate the heat fluxes at the two plates.

5.10 ***Parallel-Plate, Nonisothermal Newtonian Drag Flow with Temperature-dependent Viscosity*** (a) Review the approximate linear perturbation solution given in Example 1.2-2 in R. B. Bird, R. C. Armstrong, and O. Hassager, *Dynamics of Polymeric Fluids*, Vol. 1, Wiley, New York, 1977. (b) Review an exact analytical solution in B. Martin, *Int. J. Non-Newtonian Mech.*, **2,** 285–301 (1967).

5.11 ***Formation of Thick Polymer Sheets*** Forming thick sheets of unplasticized amorphous polymers (e.g., PVC) is difficult because of the frequency of void formation during cooling. For this reason such products are sometimes made by pressing together a number of thin extruded sheets between hot plates in hydraulic presses. (a) Using Fig. 5.8 estimate the time required to fuse together twenty sheets of PVC, each 0.05 cm thick, initially at 20°C, by pressing them between two hot plates kept at a constant temperature of 150°C. Use the thermo-physical data in Appendix A. (b) Discuss the problem of thermal degradation.

5.12 ***Cooling of Extruded PE Wire***[5] Consider a copper conductor, 0.16 in in diameter, coated by extrusion to a 0.62-in insulated wire (first transatlantic cable core wire). The conductor is preheated to the extrusion temperature 412°F, and

5. R. D. Biggs and R. P. Guenther, *Mod. Plast.*, **1963**, 126 (May 1963).

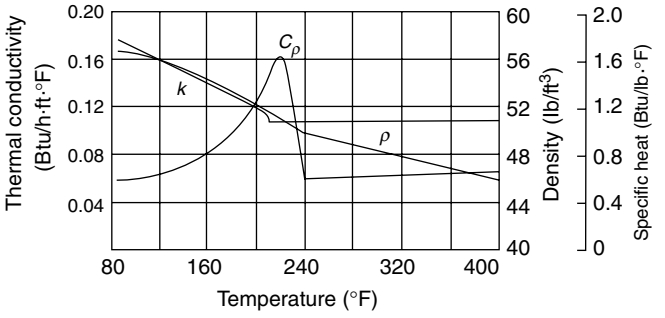

exits into a water trough maintained at 80°F at 42 ft/min. Assuming a flat temperature distribution in the copper, since its conductivity is about 2000 times that of PE, solve the heat transfer problem of cooling the insulated wire in terms of a heat-transfer coefficient of 500 (Btu/ft^2·hr·°F) and the thermophysical properties for PE shown in accompanying figure.

5.13 ***Adiabatic Compression Heating*** Melting of polymers by adiabatic compression has been shown to be feasible for processes such as injection molding (2). Discuss this method, in principle, in terms of an order-of-magnitude analysis of the terms of the thermal energy balance for an amorphous (PS) and a semicrystalline polymer (LDPE). Use the data in Appendix A.

5.14 ***Melting Efficiency with Melt Removal in Conductive Melting*** There are four reasons for melt removal (from the heat-transfer region) in conductive melting. The first is efficiency of melting; the second is avoidance of thermal degradation by shortening the residence time of the melt in regions near high-temperature surfaces; the third is the further generation of heat in the entire volume of the melt by viscous dissipation of mechanical energy; and the fourth is that melt removal induces laminar mixing and thermal homogenization. In this Problem, we wish to compare the melting efficiency and polymer melt stability for the ''melting'' of PVC with and without melt removal. A slab of PVC $8 \times 8 \times 2$ cm at 20°C is to be melted by a hot metal surface at 200°C. Melt removal is accomplished by moving the hot surface at a speed of 1 cm/s. Use data in Fig. 5.3 and Appendix A. Assume an average value for ρ, k, and C_p below and above T_g.

5.15 ***Sintering of PS "Pearls"*** Calculate the rate of coalescence of PS ''pearls'' made from suspension polymerization, which are 0.2 cm in diameter. The temperature of the sintering process is 180°C. Use the Power Law constants of the unmodified PS in Appendix A. The surface tension of the melt can be taken to be 32.4 dyne/cm.[6]

6. H. Schonhorn, ''Theory of Adhesive Joints,'' in *Adhesion and Bonding*, N. M. Bikales, Ed., Wiley, New York, 1971.

5.16 ***Flow and Heat Transfer in the Molten Film during Melt Removal*** Formulate equations of the coupled heat transfer and flow problems involved during the melt removal (by a simple shearing flow) in the conductive heating of a polymer sheet. If x is the direction of the melt removal and y the direction of the main temperature gradient, allow both v_x and v_y to be nonzero (because $\delta = \delta(x)$); also, allow for a convective heat flux in the x direction. Assume that the polymer is crystalline, with constant "average" values for ρ, k, and C_p.

5.17 ***Heat Transfer in Blow Molding*** Estimate the cooling time of a 15 cm long, 4 cm in O.D., and 0.3 cm thick HDPE parison at 200°C, which is inflated onto a 10-cm-diameter and 15-cm-long cylindrical bottle mold at 15°C by 5°C cold air. Solve the heat-transfer problem involved. Use the ρ, k, and C_p data given in Appendix A. Assume that the inner surface of the bottle is at 15°C.

5.18 ***Heat Transfer in Underwater Pelletizing*** In underwater pelletizing, the melt strands are extruded directly in a water bath and "chopped" by a rotating, high-speed knife into short-length cylinders called *pellets*. Consider an LDPE extrudate at 200°C, chopped into pellets of $L = D = 0.4$ cm in a bath kept at 10°C. (a) Formulate the complete heat-transfer problem. (b) Estimate the time required to cool the center of the pellet to 70°C by assuming that pellet surface temperature equals the temperature of the water.